

Causal Representation Learning with Generative Artificial Intelligence: Application to Texts as Treatments*

Kosuke Imai[†]Kentarō Nakamura[‡]

November 25, 2024

Abstract

In this paper, we demonstrate how to enhance the validity of causal inference with unstructured high-dimensional treatments like texts, by leveraging the power of generative Artificial Intelligence. Specifically, we propose to use a deep generative model such as large language models (LLMs) to efficiently generate treatments and use their internal representation for subsequent causal effect estimation. We show that the knowledge of this true internal representation helps disentangle the treatment features of interest, such as specific sentiments and certain topics, from other possibly unknown confounding features. Unlike the existing methods, our proposed approach eliminates the need to learn causal representation from the data and hence produces more accurate and efficient estimates. We formally establish the conditions required for the nonparametric identification of the average treatment effect, propose an estimation strategy that avoids the violation of the overlap assumption, and derive the asymptotic properties of the proposed estimator through the application of double machine learning. Finally, using an instrumental variables approach, we extend the proposed methodology to the settings, in which the treatment feature is based on human perception rather than is assumed to be fixed given the treatment object. The proposed methodology is also applicable to text reuse where an LLM is used to regenerate the existing texts. We conduct simulation and empirical studies, using the generated text data from an open-source LLM, Llama 3, to illustrate the advantages of our estimator over the state-of-the-art causal representation learning algorithms.

Key Words: causal inference, deep generative models, double machine learning, large language models, unstructured treatments

*We thank Christian Fong and Justin Grimmer for kindly sharing their dataset used in Candidate Profile Experiment and Naoki Egami for helpful comments.

[†]Professor, Department of Government and Department of Statistics, Harvard University, Cambridge, MA 02138. Phone: 617-384-6778, Email: Imai@Harvard.Edu, URL: <https://imai.fas.harvard.edu>

[‡]Ph.D. student, John F. Kennedy School of Government, Harvard University. Email: knakamura@g.harvard.edu

1 Introduction

The emergence of generative artificial intelligence (AI) technology such as large language models (LLMs) has had an enormous impact on a variety of fields, including medicine (Thirunavukarasu et al., 2023), education (Kasneji et al., 2023), marketing (Kshetri et al., 2024), and social sciences (Ludwig and Mullainathan, 2024; Bisbee et al., 2024). These AI tools come with advanced capabilities to quickly generate realistic texts, images, and videos based on prompts provided by users.

In this paper, we demonstrate that generative AI can be used to enhance the performance of causal representation learning from unstructured data. As a concrete application of the proposed methodology, we focus on the settings where texts are used as treatments. Specifically, we introduce an experimental design (Section 2) and develop an efficient estimation strategy to infer the causal effects of specific features contained in texts, such as sentiments and topics (Section 3).

In the proposed experiment, we first generate texts by providing treatment and control prompts to an LLM. If one wishes to use the existing texts as treatments rather than generate new ones to improve external validity (Egami and Hartman, 2023), we could ask an LLM to reproduce the texts exactly. We then present each of these generated texts to a randomly selected survey respondent and measure their reactions. Lastly, we directly extract the true internal representation of generated texts from the LLM and analyze it with a machine learning algorithm to disentangle treatment features from other confounding features contained within the same texts. The key insight of our proposed approach is to leverage the true vectorized representation of treatment texts that is available in an open-source deep generative model. This enables us to learn efficiently causal representation of unstructured data even when texts contain strong confounding features.

As part of the proposed estimation approach, we develop a neural network architecture based on TarNet (Shalit et al., 2017) to separately learn treatment and confounding features. We prove that it is possible to nonparametrically identify a *deconfounder*, which summarizes all confounding features as a lower-dimensional function of the internal representation obtained from a deep generative model. Once a deconfounder is estimated, we use it to model the treatment features and estimate the propensity score. We then apply the double machine learning (DML) methodology to obtain the asymptotically valid confidence intervals (Chernozhukov et al., 2018).

Lastly, we extend the proposed methodology to the estimation of the causal effects of *perceived* treatment features, motivated by the fact that respondents may perceive the same treatment features differently (Section 4). A methodological challenge is that the perceived treatment features may be confounded by possibly unobserved respondent characteristics as well as the confounding features of texts. To address this, we incorporate the instrumental variable approach (Imbens and Angrist, 1994) into our estimation approach by using the actual treatment features as instruments for their perceived counterparts.

To investigate the empirical performance of the proposed methodology, we design simulation studies based on the candidate profile experiment of Fong and Grimmer (2016) (Section 5). In this experiment, survey respondents are asked to evaluate biographies of different political candidates. Our goal is to infer the causal effects of certain features, such as military background and education levels, contained in these biographies. We use an open-source LLM, Llama 3, to generate a set of new candidate biographies and design simulation studies to compare the performance of the proposed estimator with that of state-of-the-art methods. We also have Llama 3 regenerate the existing biographies to examine the performance of the proposed methodology in the case of text reuse.

We find that the proposed estimator outperforms these competing methods, which estimate the causal representation using the existing embedding (Pryzant et al., 2021; Gui and Veitch,

2023). Specifically, the proposed estimator has a smaller bias and root mean squared error (RMSE) while its confidence interval retains a proper nominal coverage level. These findings hold up even when the sample size is relatively small and in the case of text reuse. In sum, our simulation studies demonstrate that the AI-generated true internal representation significantly improves causal representation learning.

Finally, we also apply the proposed methodology to the human responses to the candidate profile experiment (Section 6). Our analysis shows that the previous military experience of candidate does not significantly affect voter evaluation on average.

Related literature. There exist several works that estimate the causal effects of treatment features of texts. The key difference between the proposed methodology and these previous approaches is the use of generative AI in producing treatment objects. We exploit the fact that the *true* vectorized representation of generated texts can be obtained directly from open-source deep generative models. In contrast, the existing methods learn causal representation from the treatment texts in a variety of ways. For example, Fong and Grimmer (2016); Ahrens et al. (2021) impose modeling assumptions based on topic models, whereas Pryzant et al. (2021) and Gui and Veitch (2023) estimate the vector representation using the BERT (Bidirectional Encoder Representations from Transformers) embeddings. We show that the use of true representation not only improves the estimation performance but also significantly increases computational efficiency.

Our work has broader implications for the literature on causal inference and unstructured objects in general (see Feder et al., 2022, for a recent review of causal inference with texts). For example, scholars have developed methods that adjust for texts as confounders, but all of these methods estimate a low-dimensional representation of confounding information from texts (Veitch et al., 2020; Roberts et al., 2020; Klaassen et al., 2024; Mozer et al., 2020, 2024). Although our paper focuses on the use of texts as treatments rather than confounders, the proposed use of generative AI should be beneficial for these other cases where the existing estimation methods are likely to suffer from estimation error (Keith et al., 2020).

Similarly, the proposed approach may also be applicable to causal inference with images and even videos. For example, Jerzak et al. (2023a,b) have considered the use of causal inference with images in the observational setting. Given the availability of deep generative models for images, it would be of interest to use generative AI for improved causal inference with images (e.g., Ramesh et al., 2021; Rombach et al., 2022; Shrestha and Xie, 2023; Ye et al., 2023).

Our work contributes to the literature on representation learning for causal inference. Since unstructured objects like texts are fundamentally high-dimensional, learning a low-dimensional representation is crucial (e.g., Shi et al., 2019; Wang and Jordan, 2022). Some existing works on causal inference with texts learn a low-dimensional representation that predicts both the treatment and outcome well (e.g., Veitch et al., 2020; Gui and Veitch, 2023). While we also use a low-dimensional representation to adjust for confounding features, the proposed methodology disentangles confounding features from treatment features without violating the overlap assumption.

Finally, our methodology differs from that of Wang and Blei (2019) though both use the estimated “deconfounder” for confounding adjustment. Most importantly, Wang and Blei (2019) adjusts the *unobserved* confounding by estimating the deconfounder as a function of treatments (Imai and Jiang, 2019). In contrast, the goal of the proposed methodology is to learn a representation of *observed* confounding by estimating the deconfounder as a function of generative model’s internal representation of treatment objects. Under this setting, we formally establish the nonparametric identification of the average treatment effect.

Candidate biography with military background

Anthony Higgins was born in Red Lion Hundred in New Castle County, Delaware. He attended Newark Academy and Delaware College, and graduated from Yale College in 1861, where he was a member of Skull and Bones. After studying law at the Harvard Law School, he was admitted to the bar in 1864 and began practice in Wilmington, Delaware. He also served for a time in the United States Army in 1864.

Candidate biography without military background

Benjamin Tappan was born in Northampton, Massachusetts, the second child and oldest son of Benjamin Tappan and Sarah (Homes) Tappan, who was a grandniece of Benjamin Franklin. Two of his younger brothers were abolitionists Arthur Tappan and Lewis Tappan. He attended the public schools in Northampton and traveled to the West Indies in his youth. He apprenticed as a printer and engraver, also studying painting with Gilbert Stuart. He read law to be admitted to the bar in Hartford, Connecticut, in 1799. Later that year, he moved to the Connecticut Western Reserve and founded what is now Ravenna, Ohio, laying out the original village in 1808. He married, March 20, 1801, Nancy Wright, sister of John C. Wright (congressman), afterwards a United States House of Representatives from Ohio. They had one son, Benjamin, born in 1812.

Table 1: Two examples of candidate biographies with and without military background from the experiment conducted by Fong and Grimmer (2016)

2 The Experimental Design for Texts as Treatments

While the proposed methodology is general, it is helpful to consider a concrete application. Specifically, we consider the candidate profile experiment conducted and analyzed by Fong and Grimmer (2016) which investigates how various features of a political candidate affect their voter evaluation. In the context of this experiment, we describe our alternative approach that uses LLMs to generate treatment texts. In Sections 5 and 6, we return to this application to empirically evaluate the performance of the proposed methodology relative to the existing state-of-the-art methods.

2.1 Candidate profile experiment

Fong and Grimmer (2016) gathered a collection of 1,246 candidate biographies (written in texts) from Wikipedia, and then recruited a total of 1,886 voters who were asked to answer an online survey evaluating up to four randomly assigned candidate profiles. Specifically, the survey asked these voters to rate each candidate biography using a feeling thermometer that ranges from 0 (cold) to 100 (warm). The authors first used a supervised Bayesian model based on the Indian buffet process to discover a total of 10 treatment features and then estimated the marginal association between each treatment feature and the observed feeling thermometer value.

Unlike the original analysis, we consider a setting, in which researchers have a specific treatment feature of interest. Suppose that we are interested in estimating the causal effect of having a military background on voter evaluation. The relevant political science literature suggests that the experience and occupation of candidates play an important role (e.g., Kirkland and Coppock, 2018; Campbell and Cowley, 2014; Pedersen et al., 2019). Indeed, the original analysis shows that candidate biographies with military background tend to receive a high feeling thermometer score.

The methodological challenge, however, is that military background may be correlated with other features present in candidate biographies. Table 1 displays two examples of candidate biography used in the original experiment. The first biography describes a candidate with military

background whereas the second one shows another candidate without military background. Yet, these two biographies also differ in terms of other features, including educational background, marital status, and family structure. The length of each biography and their levels of details are also different. If these additional differences are correlated with military background and influence voter evaluation, then the simple comparison between biographies with military background and those without it would lead to biased causal estimates.

2.2 Using large language models to (re)generate treatment texts

We use an LLM to generate treatment texts. In the current context, we can achieve this in two ways. First, we can provide a prompt to an LLM, asking it to generate a candidate biography from scratch. Alternatively, we can use existing biographies (e.g., those collected by Fong and Grimmer (2016)) and then ask an LLM to reproduce the same biographies without any modification.

Both approaches require (1) the coding of the treatment variable (e.g., the existence of military background) and (2) the extraction of the internal representation of LLM used to generate treatment texts. The first requirement may mean that human coders have to read treatment texts unless one is willing to assume that LLM has a good compliance with the instruction in prompts. The second requirement implies that we should use open-source LLMs including GPT (Generative Pre-trained Transformer; Radford et al. 2018), PaLM (Pathways Language Model; Chowdhery et al. 2022), Llama (Large Language Model Meta AI; Touvron et al. 2023), OPT (Open Pre-trained Transformer; Zhang et al. 2022). We note that the internal representation is not accessible for OpenAI’s GPT-4, making it impossible to use ChatGPT for our purpose.

Table 2 shows an example from each approach. Here, we use Meta’s Llama 3 instruction-tuned model with eight billion parameters. This model takes two types of inputs: system-level inputs (**System**), which define the type of task to be performed, and user-level inputs (**User**), which define a specific task to be performed. The first example in the table shows how the model generates a new candidate biography with military background from scratch, whereas the second example shows how the model simply reproduces the biography that is given. The former suggests that generative models can efficiently create realistic treatments, while the latter indicates that they can follow the instruction accurately.

We emphasize that the use of LLM in itself does not solve the confounding bias automatically. This is because the LLM learns the associations of words in the real-world texts, and even if manipulate the concepts with instructions, other correlated concepts might be influenced as well, which still causes the confounding bias (Hu and Li, 2021). Now, we turn to the proposed methodology that adjusts for confounding features in unstructured treatment objects such as texts to estimate the causal effects of the specific treatment feature of interest.

3 The Proposed Methodology

In this section, we present the proposed methodology. We begin by defining the causal quantity of interest, establishing its nonparametric identification, and develop an estimation strategy.

3.1 Assumptions and causal quantity of interest

Consider a simple random sample of N respondents drawn from a population of interest. For each respondent $i = 1, 2, \dots, N$, we assign a prompt P_i that is randomly and independently sampled from a set of potential prompts \mathcal{P} . In our application, prompts are based on natural language (e.g., “Create a biography of an American politician who has some military experience”). While our framework allows for stratified randomization, for the sake of simplicity, we assume that the random assignment of prompt is done without conditioning on pre-treatment covariates such as respondent characteristics and types of prompts. Given each prompt, we use a deep generative

Prompts	Generated candidate biography
<p>(System): You are a text generator who always produces a biography of the instructed person.</p> <p>(User): Create a biography of an American politician named Nathaniel C. Gilchrist</p>	<p>Nathaniel C. Gilchrist was an American politician who served as a member of the United States House of Representatives from Maryland’s 4th congressional district from 1895 to 1899. Born on November 24, 1847, in Baltimore, Maryland, Gilchrist was the son of a prominent family of merchants and shipbuilders. He was educated at the Baltimore City College and later attended the University of Maryland, where he studied law. After graduating, he was admitted to the bar and began practicing law in Baltimore.</p>
<p>(System): You are a text generator who just repeats the input text.</p> <p>(User): Higgins was born in Red Lion Hundred in New Castle County, Delaware. He attended Newark Academy and Delaware College, and graduated from Yale College in 1861, where he was a member of Skull and Bones. After studying law at the Harvard Law School, he was admitted to the bar in 1864 and began practice in Wilmington, Delaware. He also served for a time in the United States Army in 1864.</p>	<p>Higgins was born in Red Lion Hundred in New Castle County, Delaware. He attended Newark Academy and Delaware College, and graduated from Yale College in 1861, where he was a member of Skull and Bones. After studying law at the Harvard Law School, he was admitted to the bar in 1864 and began practice in Wilmington, Delaware. He also served for a time in the United States Army in 1864.</p>

Table 2: Two examples of generated candidate biographies with Llama 3. The system-level input (**System**) defines the type of tasks to be performed, whereas the user-level input (**User**) defines a specific task to be performed.

model to generate a *treatment object*, which is denoted by $\mathbf{X}_i \in \mathcal{X}$ where \mathcal{X} is the support of \mathbf{X}_i . These treatment objects are typically high-dimensional and unstructured and, in our application, they are texts.

We use a broad definition of a deep generative model so that it can encompass many LLMs and other types of foundation models. For example, our definition includes a number of models for texts (e.g., Keskar et al., 2019; Yang and Klein, 2021; Guo et al., 2022; Zhou et al., 2023; Chowdhery et al., 2022; Radford et al., 2018; Touvron et al., 2023; Zhang et al., 2022; Jiang et al., 2023).

DEFINITION 1 (DEEP GENERATIVE MODEL) *A deep generative model is the following probabilistic model that takes prompt \mathbf{P}_i as an input and generates the treatment object \mathbf{X}_i as an output:*

$$\mathbb{P}(\mathbf{X}_i \mid \mathbf{h}_\gamma(\mathbf{R}_i))$$

$$\mathbb{P}(\mathbf{R}_i \mid \mathbf{P}_i)$$

where $\mathbf{R}_i \in \mathbb{R}^r$ denotes an observable internal representation of \mathbf{X}_i contained in the model and $\mathbf{h}_\gamma(\mathbf{R}_i)$ is a deterministic function parameterized by γ that completely characterizes the conditional distribution of \mathbf{X}_i given \mathbf{R}_i .

Under this definition of deep generative model, \mathbf{R} represents a lower-dimensional representation of treatment object \mathbf{X} and is a hidden representation of neural networks. In addition, $\mathbf{h}_\gamma(\mathbf{R})$ is the propensity function (Imai and Van Dyk, 2004) and is both known and observable in an open-source deep generative model. Thus, under this deep generative model, the treatment object \mathbf{X} only depends on \mathbf{P} through $\mathbf{h}_\gamma(\mathbf{R})$.

In the proposed experiment, each respondent i is exposed to the generated treatment object \mathbf{X}_i , and subsequently yields the outcome variable $Y_i \in \mathcal{Y} \subset \mathbb{R}$ where \mathcal{Y} is the support of Y_i . In our application, the treatment object is a candidate biography and the outcome is a respondent’s evaluation of the biography. Let $Y_i(\mathbf{x})$ represent the potential outcome of respondent i when exposed to a treatment object $\mathbf{x} \in \mathcal{X}$. Then, the observed outcome is solely determined by the assigned treatment object, i.e., $Y_i = Y_i(\mathbf{X}_i)$. This notation assumes no interference between units and no hidden multiple version of treatment object (Rubin, 1990). This experimental design implies the following two assumptions.

ASSUMPTION 1 (CONSISTENCY) *The potential outcome under the treatment object $\mathbf{x} \in \mathcal{X}$ is denoted by $Y_i(\mathbf{x})$ and equals the observed outcome Y_i under the realized treatment object \mathbf{X}_i :*

$$Y_i = Y_i(\mathbf{X}_i).$$

ASSUMPTION 2 (RANDOM ASSIGNMENT OF PROMPT) *Prompt is randomly assigned such that the following independence holds for all i and $\mathbf{x} \in \mathcal{X}$:*

$$Y_i(\mathbf{x}) \perp\!\!\!\perp \mathbf{P}_i.$$

We are interested in estimating the causal effect of a particular feature that can be part of a treatment object. For simplicity, we consider a binary treatment feature denoted by $T_i \in \{0, 1\}$ for each i . In our application, $T_i = 1$ if candidate biography i contains some military background and $T_i = 0$ otherwise. We assume that the treatment feature T is determined solely by the treatment object \mathbf{X} .

ASSUMPTION 3 (TREATMENT FEATURE) *There exists a deterministic function $g_T : \mathcal{X} \rightarrow \{0, 1\}$ that maps a treatment object \mathbf{X}_i to a binary treatment feature of interest $T_i \in \{0, 1\}$, i.e.,*

$$T_i = g_T(\mathbf{X}_i).$$

The function g_T is called the “codebook function” in the literature (Egami et al., 2022). This assumption is violated, for example, if respondents infer different values of the treatment feature from the same treatment object. We address this issue in Section 4 by considering the perceived treatment, which reflects the heterogeneity across respondents.

Next, we define the confounding features, which represent all features of \mathbf{X} other than the treatment feature T that influence outcome Y . These confounding features, denoted by \mathbf{U}_i , are based on a vector-valued deterministic function of \mathbf{X} and are denoted by $\mathbf{U} \in \mathcal{U}$ where \mathcal{U} denotes their support. The confounding features may be multiple dimensional though we assume its dimensionality is much smaller than that of treatment object. In our application, the confounding features may include other candidate background and characteristics as well as textual features of biographies such as their length. These confounding features are possibly correlated with the treatment feature. Unlike the treatment feature, however, we do not completely observe the confounding features. Formally, the confounding features are defined as follows.

ASSUMPTION 4 (CONFOUNDING FEATURES) *There exists a unknown deterministic vector-valued function $\mathbf{g}_U : \mathcal{X} \rightarrow \mathcal{U}$ that maps an unstructured object $\mathbf{X}_i \in \mathcal{X}$ to the confounding features $\mathbf{U}_i \in \mathcal{U}$, i.e.,*

$$\mathbf{U}_i = \mathbf{g}_U(\mathbf{X}_i),$$

where $\dim(\mathbf{U}_i) \ll \dim(\mathbf{X}_i)$.

The confounding features are also introduced as a deterministic function of treatment objects in the existing literature on causal inference with texts (Fong and Grimmer, 2023; Pryzant et al., 2021).

Finally, we assume that the potential outcome is a function of treatment and confounding features and that we can intervene the treatment feature without changing the confounding features. In other words, the treatment feature is not a deterministic function of the confounding features. The confounding features should not be a function of treatment because we only want to control pre-treatment variables (Daoud et al., 2022). In the candidate biography application, the assumption essentially implies that researchers need to be able to imagine hypothetical candidate biographies with and without military background while keeping the confounding features constant. We formalize this assumption as follows.

ASSUMPTION 5 (SEPARABILITY OF TREATMENT AND CONFOUNDING FEATURES) *The potential outcome is a function of the treatment feature of interest t and another separate function of the confounding features \mathbf{u} . That is, for any given $\mathbf{x} \in \mathcal{X}$ and all i , we have:*

$$Y_i(\mathbf{x}) = Y_i(t, \mathbf{u}) = Y_i(g_T(\mathbf{x}), \mathbf{g}_U(\mathbf{x})),$$

where $t = g_T(\mathbf{x}) \in \{0, 1\}$ and $\mathbf{u} = \mathbf{g}_U(\mathbf{x}) \in \mathcal{U}$. In addition, g_T and \mathbf{g}_U are separable such that there exist no function \tilde{g} and $\tilde{\mathbf{g}}$ such that $g_T(\mathbf{x}) = \tilde{g} \circ \mathbf{g}_U(\mathbf{x})$ or $\mathbf{g}_U(\mathbf{x}) = \tilde{\mathbf{g}} \circ g_T(\mathbf{x})$ for some $\mathbf{x} \in \mathcal{X}$.

Importantly, Assumptions 3–5 imply the standard overlap condition in causal inference. We state this as the following lemma.

LEMMA 1 (OVERLAP) *Under Assumptions 3–5, for any $t \in \{0, 1\}$ and $\mathbf{u} \in \mathcal{U}$,*

$$\mathbb{P}(T_i = t \mid \mathbf{U}_i = \mathbf{u}) > 0.$$

Proof is given in Appendix S1.1.

Under this setup, we are interested in estimating the average causal effect of the treatment feature while controlling for the confounding features. This average treatment effect (ATE) is defined as follows:

$$\tau := \mathbb{E}[Y_i(1, \mathbf{U}_i) - Y_i(0, \mathbf{U}_i)]. \quad (1)$$

This estimand is similar to the average marginal component effect (AMCE) in conjoint analysis (Hainmueller et al., 2014; Egami and Imai, 2019). Unlike conjoint experiments, however, the confounding features are unstructured, unknown, and not independent of the treatment feature.

3.2 Nonparametric identification

Figure 1 presents a directed acyclic graph (DAG) that summarizes the data generating process and assumptions described above. In this DAG, an arrow with double lines represents a deterministic causal relation while an arrow with a single line indicates a possibly stochastic causal relationship. We consider a deep generative model whose decoding is deterministic, meaning that the output text is a deterministic function of the input prompt. Formally, we make the following assumption.

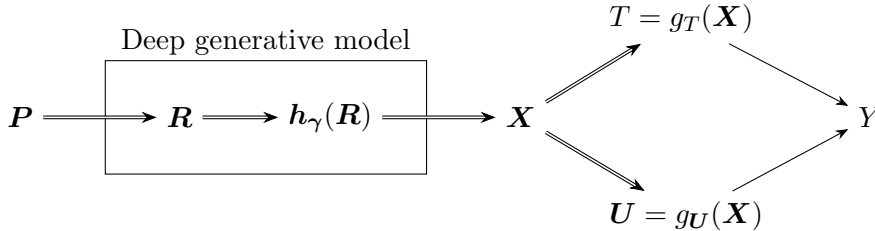


Figure 1: Directed Acyclic Graph of the Assumed Data Generating Process. A treatment object \mathbf{X} (e.g., texts) is generated using a deep generative model (rectangle), in which a prompt \mathbf{P} produces an internal representation \mathbf{R} that generates \mathbf{X} through a propensity function $\mathbf{h}_\gamma(\mathbf{R})$. The treatment object affects the outcome Y through its treatment feature of interest T and other confounding features \mathbf{U} . An arrow with double lines represents a deterministic causal relation while an arrow with a single line indicates a possibly stochastic relationship.

ASSUMPTION 6 (DETERMINISTIC DECODING) *The output layer of a deep generative model is deterministic. That is, both $\mathbb{P}(\mathbf{X}_i | \mathbf{h}_\gamma(\mathbf{R}_i))$ and $\mathbb{P}(\mathbf{R}_i | \mathbf{P}_i)$ in Definition 1 are degenerate distributions.*

Without this assumption, a deep generative model may induce dependency between observations, complicating statistical inference. In addition, if $\mathbb{P}(\mathbf{X}_i | \mathbf{h}_\gamma(\mathbf{R}_i))$ is stochastic, the noise introduced by the deep generative model may confound the treatment in an unknown way. Fortunately, almost all language models satisfy this assumption as they have an option of deterministic decoding including greedy, beam, or contrastive searches. Thus, the assumption can be easily satisfied by changing the hyperparameter of generative model. For example, for greedy decoding, we typically only need to set the temperature parameter to zero, instructing a deep generative model to always produce the same texts (e.g., Su et al., 2022). Nevertheless, some deep generative models do not satisfy Assumption 6. They include diffusion and score-based generative models without deterministic sampling, which is used to generate images and videos (e.g., Ho et al., 2020; Song et al., 2020).

Given this setup, we establish the nonparametric identification of the ATE defined in Equation (1). Specifically, we prove that there exists a deconfounder function $\mathbf{f}(\mathbf{R}_i)$, satisfying the conditional independence relation $Y_i \perp\!\!\!\perp \mathbf{R}_i | T_i, \mathbf{f}(\mathbf{R}_i)$. One trivial example of the deconfounder is the confounding features \mathbf{U}_i , which are a deterministic function of \mathbf{R}_i under Assumption 6, but the deconfounder need not be unique. In fact, we show that it is possible to identify the ATE by adjusting for any deconfounder.

THEOREM 1 (NONPARAMETRIC IDENTIFICATION OF THE MARGINAL DISTRIBUTION OF POTENTIAL OUTCOME) *Under Assumptions 1–6, there exists a deconfounder function $\mathbf{f} : \mathbb{R}^r \rightarrow \mathbb{R}^q$ with $q \leq r$ that satisfies the following conditional independence relation:*

$$Y_i \perp\!\!\!\perp \mathbf{R}_i | T_i = t, \mathbf{f}(\mathbf{R}_i), \quad (2)$$

for $t = 0, 1$. By adjusting for this deconfounder, we can nonparametrically identify the marginal distribution of potential outcome under the treatment condition $T_i = t$ for $t \in \{0, 1\}$ as:

$$\mathbb{P}(Y_i(t, \mathbf{U}_i) = y) = \int_{\mathbb{R}^r} \mathbb{P}(Y_i = y | T_i = t, \mathbf{f}(\mathbf{R}_i)) dF(\mathbf{R}_i),$$

where $y \in \mathcal{Y}$.

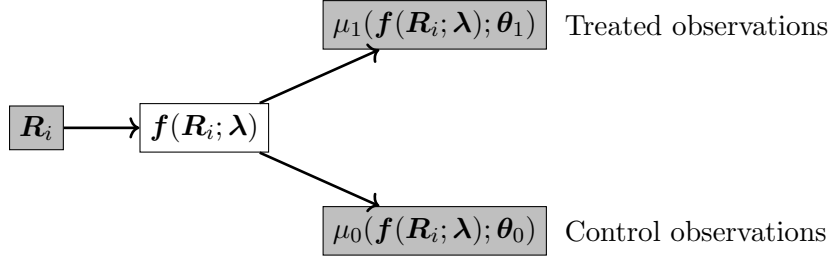


Figure 2: Diagram Illustrating the Proposed Model Architecture. The proposed model takes an internal representation of a treatment object \mathbf{R}_i as an input, and finds a deconfounder $\mathbf{f}(\mathbf{R}_i)$, which is a lower-dimensional representation of \mathbf{R}_i , and then use it to predict the conditional expectation of the outcome $\mu_t(\mathbf{f}(\mathbf{R}_i)) := \mathbb{E}[Y_i | T_i = t, \mathbf{f}(\mathbf{R}_i)]$ under each treatment arm $t = 0, 1$.

Proof is given in Appendix S1.2.

We emphasize that one cannot directly adjust for the internal representation of treatment object, i.e., \mathbf{R}_i . Such direct adjustment leads to the lack of overlap because, under Assumptions 3 and 6, the treatment feature T_i is a deterministic function of \mathbf{R}_i . In addition, since the deconfounder $\mathbf{f}(\mathbf{R}_i)$ is typically of much lower dimension than the internal representation of treatment object \mathbf{R}_i , making adjustments for the former leads to a more effective estimation strategy than directly adjusting for the latter.

3.3 Estimation and inference

Given the identification result, we next consider estimation and inference. Our estimation strategy is based on the following two observations. First, Assumption 5 implies that the deconfounder $\mathbf{f}(\mathbf{R}_i)$ should not be a function of treatment feature T_i . Second, the deconfounder should satisfy the conditional independence relation given in Equation (2).

We use a neural network architecture based on TarNet (Shalit et al., 2017) to estimate the conditional potential outcome function given the deconfounder, i.e.,

$$\mu_t(\mathbf{f}(\mathbf{R}_i)) := \mathbb{E}[Y_i(t, \mathbf{U}_i) | \mathbf{f}(\mathbf{R}_i)], \quad \text{for } t = 0, 1.$$

Our architecture, which is summarized in Figure 2, simultaneously estimates the deconfounder and the outcome model. Specifically, we minimize the following loss function:

$$\{\hat{\boldsymbol{\lambda}}, \hat{\boldsymbol{\theta}}_0, \hat{\boldsymbol{\theta}}_1\} = \underset{\boldsymbol{\lambda}, \boldsymbol{\theta}_0, \boldsymbol{\theta}_1}{\operatorname{argmin}} \frac{1}{n} \sum_{i=1}^n \{Y_i - \mu_{T_i}(\mathbf{f}(\mathbf{R}_i; \boldsymbol{\lambda}); \boldsymbol{\theta}_{T_i})\}^2, \quad (3)$$

where n is the sample size. We make the parameters of neural network explicit by letting $\boldsymbol{\lambda}$ represent the parameters of deconfounder \mathbf{f} to be estimated, and using $\boldsymbol{\theta}_t$ to denote the parameters of the nuisance function μ_t .

Given the above architecture, we estimate the ATE using the double machine learning (DML) framework of Chernozhukov et al. (2018), in which both the outcome and propensity score models are estimated. Here, we propose to estimate the propensity score model as a function of the estimated deconfounder, i.e., $\pi(\mathbf{f}(\mathbf{R}_i; \hat{\boldsymbol{\lambda}})) = \Pr(T_i = 1 | \mathbf{f}(\mathbf{R}_i; \hat{\boldsymbol{\lambda}}))$ after solving the minimization problem in Equation (3). Importantly, we do not model the propensity score as a function of internal representation \mathbf{R}_i in order to avoid the violation of the overlap assumption.

In the literature on causal representation learning, DragonNet (Shi et al., 2019) is a popular method of estimation used by many researchers (see e.g., Veitch et al., 2020; Gui and Veitch, 2023, as well as Pryzant et al. 2021 who also use it in their implementation code). Unlike our approach,

DragonNet includes the cross-entropy loss between the propensity score model and the treatment variable when estimating the deconfounder $\mathbf{f}(\mathbf{R}_i)$. However, this joint estimation leads to $\mathbb{P}(T_i = 1 \mid \mathbf{f}(\mathbf{R}_i)) = \mathbb{P}(T_i = 1 \mid \mathbf{R}_i)$ due to the fact that $\mathbf{f}(\mathbf{R}_i)$ is a balancing score satisfying $T_i \perp\!\!\!\perp \mathbf{R}_i \mid \mathbf{f}(\mathbf{R}_i)$. This is problematic because $\mathbb{P}(T_i = 1 \mid \mathbf{R}_i)$ is degenerate under Assumptions 3 and 6. Thus, we first estimate the deconfounder via Equation (3) and then model the propensity score given the estimated deconfounder.

In sum, the entire estimation procedure can be described as follows. Denote the observed data by $\mathcal{D} := \{\mathcal{D}_i\}_{i=1}^N$ where $\mathcal{D}_i := \{Y_i, T_i, \mathbf{R}_i\}$. We use the following K -fold cross-fitting procedure, assuming that N is divisible by K .

1. Randomly partition the data into K folds of equal size where the size of each fold is $n = N/K$. The observation index is denoted by $I(i) \in \{1, \dots, K\}$ where $I(i) = k$ implies that the i th observation belongs to the k th fold.
2. For each fold $k \in \{1, \dots, K\}$, use observations with $I(i) \neq k$ as training data:
 - (a) split the training data into two folds, $I_1^{(-k)}$ and $I_2^{(-k)}$
 - (b) simultaneously obtain an estimated deconfounder and an estimated conditional outcome function on the first fold, which are denoted by $\hat{\mathbf{f}}^{(-k)}(\{\mathbf{R}_i\}_{i \in I_1^{(-k)}}) := \mathbf{f}(\{\mathbf{R}_i\}_{i \in I_1^{(-k)}}; \hat{\boldsymbol{\lambda}}^{(-k)})$ and $\hat{\mu}_t^{(-k)}(\{\mathbf{R}_i\}_{i \in I_1^{(-k)}}) := \mu_t(\mathbf{f}(\{\mathbf{R}_i\}_{i \in I_1^{(-k)}}; \hat{\boldsymbol{\lambda}}^{(-k)}); \hat{\boldsymbol{\theta}}^{(-k)})$, respectively, by solving the optimization problem given in Equation (3), and
 - (c) obtain an estimated propensity score given the estimated deconfounder on the second fold, which is denoted by $\hat{\pi}^{(-k)}(\hat{\mathbf{f}}^{(-k)}(\{\mathbf{R}_i\}_{i \in I_2^{(-k)}})) := \hat{\pi}^{(-k)}(\mathbf{f}(\{\mathbf{R}_i\}_{i \in I_2^{(-k)}}; \hat{\boldsymbol{\lambda}}^{(-k)}))$.
3. Compute the ATE estimator $\hat{\tau}$ as a solution to:

$$\frac{1}{nK} \sum_{k=1}^K \sum_{i: I(i)=k} \psi(\mathcal{D}_i; \hat{\tau}, \hat{\mathbf{f}}^{(-k)}, \mu_1^{(-k)}, \mu_0^{(-k)}, \hat{\pi}^{(-k)}) = 0, \quad (4)$$

where

$$\begin{aligned} & \psi(\mathcal{D}_i; \tau, \mathbf{f}, \mu_1, \mu_0, \pi) \\ &= \frac{T_i \{Y_i - \mu_1(\mathbf{f}(\mathbf{R}_i))\}}{\pi(\mathbf{f}(\mathbf{R}_i))} - \frac{(1 - T_i) \{Y_i - \mu_0(\mathbf{f}(\mathbf{R}_i))\}}{1 - \pi(\mathbf{f}(\mathbf{R}_i))} + \mu_1(\mathbf{f}(\mathbf{R}_i)) - \mu_0(\mathbf{f}(\mathbf{R}_i)) - \tau. \end{aligned} \quad (5)$$

To derive the asymptotic properties of the proposed estimator, we assume the following regularity conditions.

ASSUMPTION 7 (REGULARITY CONDITIONS) *Let c_1 , c_2 , and $q > 2$ be positive constants and δ_n be a sequence of positive constants approaching zero as the sample size n increases. Then, the following conditions hold.*

(a) *(Primitive conditions)*

$$\mathbb{E}[|Y_i|^q]^{1/q} \leq c_1, \quad \sup_{\mathbf{r} \in \mathcal{R}} \mathbb{E}[|Y_i - \mu_{T_i}(\mathbf{f}(\mathbf{r}))|^2 \mid \mathbf{R}_i = \mathbf{r}] \leq c_1, \quad \mathbb{E}[|Y_i - \mu_{T_i}(\mathbf{f}(\mathbf{R}_i))|^2]^{1/2} \geq c_2.$$

(b) *(Outcome model estimation)*

$$\mathbb{E}[|\hat{\mu}_{T_i}(\hat{\mathbf{f}}(\mathbf{R}_i)) - \mu_{T_i}(\mathbf{f}(\mathbf{R}_i))|^q]^{1/q} \leq c_1, \quad \mathbb{E}[|\hat{\mu}_{T_i}(\hat{\mathbf{f}}(\mathbf{R}_i)) - \mu_{T_i}(\mathbf{f}(\mathbf{R}_i))|^2]^{1/2} \leq \delta_n n^{-1/4}.$$

(c) (Deconfounder estimation)

$$\mathbb{E} \left[\left[\left\| \hat{\mathbf{f}}(\mathbf{R}_i) - \mathbf{f}(\mathbf{R}_i) \right\|^q \right]^{1/q} \leq c_1, \quad \mathbb{E} \left[\left[\left\| \hat{\mathbf{f}}(\mathbf{R}_i) - \mathbf{f}(\mathbf{R}_i) \right\|^2 \right]^{1/2} \leq \delta_n n^{-1/4} \right.$$

(d) (Propensity score estimation) $\pi(\cdot)$ is Lipschitz continuous at the every point of its support, and satisfies:

$$\mathbb{E} [|\hat{\pi}(\mathbf{f}(\mathbf{R}_i)) - \pi(\mathbf{f}(\mathbf{R}_i))|^q]^{1/q} \leq c_1, \quad \mathbb{E} [|\hat{\pi}(\mathbf{f}(\mathbf{R}_i)) - \pi(\mathbf{f}(\mathbf{R}_i))|^2]^{1/2} \leq \delta_n n^{-1/4}.$$

Like the standard application of DML (Chernozhukov et al., 2018), the required rate for nonparametric estimation of nuisance models is slower than the usual parametric estimation rate of $n^{-1/2}$. Recall that we use neural networks for the joint estimation of outcome model and deconfounder. The required convergence rate of $n^{-1/4}$ is achievable with the standard neural network architecture (Farrell et al., 2021). The propensity score function can be estimated using various nonparametric methods, including the feedforward neural networks with regularization to ensure Lipschitz continuity (Gouk et al., 2021) and the kernel-based methods with nonexpansive kernels (van Waarde and Sepulchre, 2022).

Given the above assumptions, the asymptotic normality of the proposed ATE estimator follows immediately from the DML theory.

THEOREM 2 (ASYMPTOTIC NORMALITY OF THE ATE ESTIMATOR) *Under Assumptions 1–7, the estimator $\hat{\tau}$ obtained from the influence function ψ satisfies asymptotic normality:*

$$\frac{\sqrt{n}(\hat{\tau} - \tau)}{\sigma} \xrightarrow{d} \mathcal{N}(0, 1)$$

where $\sigma^2 = \mathbb{E}[\psi(\mathcal{D}_i; \tau, \mathbf{f}, \mu_1, \mu_0, \pi)^2]$.

Proof is on Appendix S1.3. We can consistently estimate the asymptotic variance using the plugin estimator based on Equation (5).

3.4 Practical implementation details

We discuss some important details when implementing the proposed methodology in practice. First, as formally stated above in Assumption 6, researchers must choose a deep generative model that has an option of deterministic decoding. Aside from appropriately setting hyper-parameters of LLM, the assumption also implies that we should not use batches with LLMs, which may induce unknown correlations across observations. The use of LLMs that have memory should also be avoided.

In addition, the effective implementation of the proposed estimation method requires a careful choice of dimension-reduction strategy for the internal representation as well as the hyperparameter tuning for TarNet. First, the internal representation, which typically corresponds to the last hidden states of a deep generative model, is of high dimension, given by a matrix of size equal to the length of texts \times the size of representation for each token. This equals 768 for BERT-base, 1024 for BERT-large and T5-3B, and 4096 for Llama3-8B. As a result, we must apply a pooling operation and obtain a lower dimensional vector.

The type of pooling strategy depends on the architecture of a deep generative model. For example, in BERT, the first special classification token [CLS] contains the entire semantic information (Devlin et al., 2019). Thus, one could use the hidden states that correspond to this [CLS] token

alone. In BART (Bidirectional and Auto-Regressive Transformers), the special token is added at the end, so researchers might extract the hidden states of the last token (Lewis et al., 2020). In contrast, encoder-decoder models like T5 (Text-to-Text Transfer Transformer, Raffel et al. 2023) do not have such special tokens, and mean pooling is often applied (e.g., Ni et al. 2021). For decoder-only models, such as Llama (Touvron et al., 2023), the autoregressive structure forces all tokens to pay attention only to the past tokens, and hence, we can use the hidden states of the last token.

Second, for TarNet, we must carefully choose hyperparameters such as the size and depth of layers, learning rate, and maximum epoch size. Together, they determine the success of optimization and the quality of deconfounder estimate. The dimension of the deconfounder should be sufficiently large to capture the confounding information but should not be too large to violate the overlap assumption. The learning rate and epoch size are also crucial, as the performance of the proposed methodology depends heavily on the success of the optimization process. As a practical strategy, researchers could try several different values of hyperparameters and select the one that minimizes the loss. If the loss does not decrease within the first few epochs, it is likely that optimization has failed. In such cases, we recommend that researchers try different sets of hyperparameters. This can be done with the advanced automatic hyperparameter optimization methods, such as Optuna (Akiba et al., 2019), that search the optimal hyperparameters automatically and efficiently by dynamically constructing the search space.

4 Instrumental Variable Approach to the Perceived Treatment Feature

The methodology described in the previous section enables the estimation of the average causal effect of the treatment feature, which is assumed to be a deterministic function of treatment object. In some cases, however, researchers may be interested in the causal effect of *perceived* treatment feature, which may not necessarily coincide with the treatment feature itself. In addition, the perception of the same treatment feature may vary across respondents. For example, in our application, respondents may disagree as to what constitutes as a military background.

In this section, we extend the proposed methodology to the setting, in which the treatment feature is used as an instrumental variable for the perceived treatment feature. As before, we describe the required assumptions, establish nonparametric identification, and propose estimation and inference strategies.

4.1 Assumptions and causal quantity of interest

We consider the same setting as in Section 3 except that we observe the perceived treatment feature $\tilde{T}_i \in \{0, 1\}$, which may not equal the treatment feature itself, i.e., $\tilde{T}_i \neq T_i$ for some i . We assume that a respondent’s perceived treatment feature is a function of the treatment and confounding features of the assigned treatment object.

ASSUMPTION 8 (PERCEIVED TREATMENT FEATURE) *The perceived treatment feature $\tilde{T}_i \in \{0, 1\}$ is a function of treatment and confounding features, i.e.,*

$$\tilde{T}_i = \tilde{T}_i(T_i, \mathbf{U}_i),$$

where $\tilde{T}_i(t, \mathbf{u})$ is the potential value of the perceived treatment feature when the treatment variable T_i is equal to $t \in \{0, 1\}$ and the confounding variables \mathbf{U}_i equal $\mathbf{u} \in \mathcal{U}$.

Importantly, under Assumption 8, different respondents may perceive the same treatment feature differently. In addition, it is also possible for the confounding features to affect the perceived

treatment feature. In practice, researchers may measure the perceived treatment feature by directly asking respondents. However, doing so may lead to the so-called *priming bias*, in which the act of asking this question itself draws a respondent’s attention to the treatment feature and confounds the causal effect of interest. To avoid this bias, researchers may measure the perceived treatment feature after the outcome variable is realized. Addressing this methodological issue is beyond the scope of this paper, but interested readers should consult a recent literature on the topic (see e.g., Montgomery et al., 2018; Aronow et al., 2019; Klar et al., 2020; Blackwell et al., 2023).

To identify the causal effect of perceived treatment feature, we use the treatment feature as an instrumental variable. To do this, we define the potential outcome as a function of the perceived treatment feature, and the treatment and confounding features. Formally, we replace Assumption 5 with the following new separability assumption.

ASSUMPTION 9 (SEPARABILITY WITH THE PERCEIVED TREATMENT FEATURE) *The potential outcome is a function of the perceived treatment \tilde{T}_i , the treatment features of interest T_i , and the confounding features \mathbf{U}_i . That is, for any given $\mathbf{x} \in \mathcal{X}$ and all i , we have:*

$$Y_i(\mathbf{x}) = Y_i(\tilde{T}_i(g_T(\mathbf{x}), \mathbf{g}_U(\mathbf{x})), g_T(\mathbf{x}), \mathbf{g}_U(\mathbf{x}))$$

where $\tilde{T}_i(g_T(\mathbf{x}), \mathbf{g}_U(\mathbf{x})) \in \{0, 1\}$ is the perceived treatment feature, $g_T(\mathbf{x}) \in \{0, 1\}$, and $\mathbf{g}_U(\mathbf{x}) \in \mathcal{U}$. In addition, g_T and \mathbf{g}_U are separable in a sense that there exist no function \tilde{g} such that $g_T(\mathbf{x}) = \tilde{g} \circ \mathbf{g}_U(\mathbf{x})$ or $\mathbf{g}_U(\mathbf{x}) = \tilde{\mathbf{g}} \circ g_T(\mathbf{x})$ for some $\mathbf{x} \in \mathcal{X}$.

Lastly, we adopt the standard instrumental variable assumptions to the current settings (Imbens and Angrist, 1994). First, we assume monotonicity; the existence of treatment feature makes it no less likely for a respondent to perceive it as such. Second, we assume exclusion restriction; the treatment feature only affects the outcome through the perceived treatment feature. Both assumptions are made while holding the confounding features constant. We formally state these assumptions here.

ASSUMPTION 10 (VALIDITY OF THE INSTRUMENTAL VARIABLE) *We make the following instrumental variable assumptions:*

(a) *(Monotonicity) For any $\mathbf{u} \in \mathcal{U}$, we have:*

$$\tilde{T}_i(1, \mathbf{u}) \geq \tilde{T}_i(0, \mathbf{u}) \quad \text{and} \quad \mathbb{P}(\tilde{T}_i(1, \mathbf{u}) = 1) > \mathbb{P}(\tilde{T}_i(0, \mathbf{u}) = 1).$$

(b) *(Exclusion Restriction) For any $\tilde{t} \in \{0, 1\}$, $\mathbf{u} \in \mathcal{U}$, and $i = 1, 2, \dots, n$, we have:*

$$Y_i(\tilde{t}, 1, \mathbf{u}) = Y_i(\tilde{t}, 0, \mathbf{u}) = Y_i(\tilde{t}, \mathbf{u}).$$

In many practical settings, the monotonicity assumption is reasonable. In our application, for example, if there is no military background in a candidate biography, a respondent should not notice the presence of this treatment feature. Exclusion restriction, however, may not be credible in some cases because it is possible for a respondent to be influenced by the treatment feature without noticing it.

Under this setup, we are interested in estimating the local average treatment effect (LATE) of the perceived treatment feature among the respondents who notice the presence of the treatment feature only when the treatment object actually contains such a feature. We define this LATE as follows:

$$\beta := \mathbb{E}[Y_i(1, \mathbf{U}_i) - Y_i(0, \mathbf{U}_i) \mid \tilde{T}_i(1, \mathbf{U}_i) = 1, \tilde{T}_i(0, \mathbf{U}_i) = 0], \quad (6)$$

where the first input of the potential outcome is the perceived treatment feature instead of the treatment feature, i.e., $Y_i(\tilde{T}_i = \tilde{t}, \mathbf{U}_i = \mathbf{u})$.

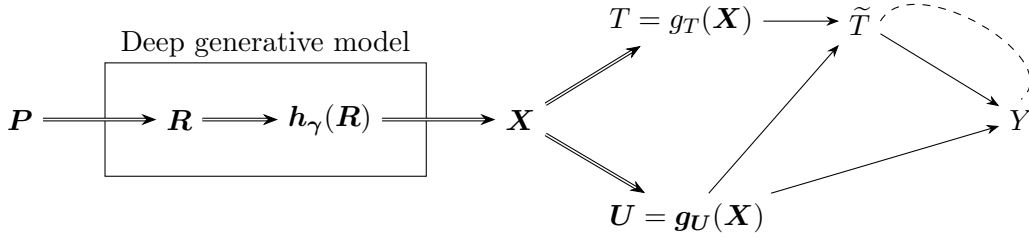


Figure 3: Directed Acyclic Graph (DAG) of the Assumed Data Generating Process with the Perceived Treatment Feature. This DAG is identical to that of Figure 1 except that the perceived treatment feature \tilde{T} is added. The perceived treatment feature may be affected by the treatment feature T and/or the confounding features \mathbf{U} . There may also be unobserved confounding variables that affect both the perceived treatment feature and the outcome Y . An arrow with double lines represents a deterministic causal relation while an arrow with a single line indicates a possibly stochastic relationship.

4.2 Nonparametric identification

We extend our nonparametric identification result obtained in Section 3.2 to the instrumental variable setting. Figure 3 summarizes the assumed data-generating process with the perceived treatment feature. The absence of direct arrow from the treatment feature T into Y encodes exclusion restriction (Assumption 10(b)). In addition, we allow for the possible existence of unobserved confounders between the perceived treatment feature and the outcome, indicated by the dotted line in the DAG.

The following theorem establishes the nonparametric identification of the LATE defined in Equation (6). As in the case of the ATE (see Theorem 1), the identification is achieved by adjusting for the deconfounder $\mathbf{f}(\mathbf{R}_i)$ and using the treatment feature T_i as an instrument for the perceived treatment feature. Similar to the ATE case, the deconfounder satisfies the conditional independence relation $\{Y_i, \tilde{T}_i\} \perp\!\!\!\perp \mathbf{R}_i \mid T_i = t, \mathbf{f}(\mathbf{R}_i)$. The difference is that the inner representation \mathbf{R}_i is now independent of the perceived treatment feature as well as the outcome after conditioning on the treatment feature and the deconfounder. Finally, we emphasize that like Theorem 1, this result does not require the deconfounder to be unique.

THEOREM 3 (NONPARAMETRIC IDENTIFICATION OF THE LATE) *Under Assumptions 1–4, 6, 8–10, there exists a deconfounder function $\mathbf{f} : \mathbf{R}^r \rightarrow \mathbf{R}^q$ with $q \leq r$ that satisfies the following conditional independence relation:*

$$\{Y_i, \tilde{T}_i\} \perp\!\!\!\perp \mathbf{R}_i \mid T_i = t, \mathbf{f}(\mathbf{R}_i),$$

for $t = 0, 1$. Then, by adjusting for this deconfounder, we can nonparametrically identify the local average treatment effect (LATE) defined in Equation (6) as:

$$\beta = \frac{\int_{\mathbb{R}^r} \mathbb{E}[Y_i \mid T_i = 1, \mathbf{f}(\mathbf{R}_i)] - \mathbb{E}[Y_i \mid T_i = 0, \mathbf{f}(\mathbf{R}_i)] dF(\mathbf{R}_i)}{\int_{\mathbb{R}^r} \mathbb{E}[\tilde{T}_i \mid T_i = 1, \mathbf{f}(\mathbf{R}_i)] - \mathbb{E}[\tilde{T}_i \mid T_i = 0, \mathbf{f}(\mathbf{R}_i)] dF(\mathbf{R}_i)}.$$

Proof is given in Appendix S1.4.

4.3 Estimation and inference

We next extend the estimation and inference approaches developed in Section 3.3 to the instrumental variable setting. The main difference is that we additionally model the conditional expectation

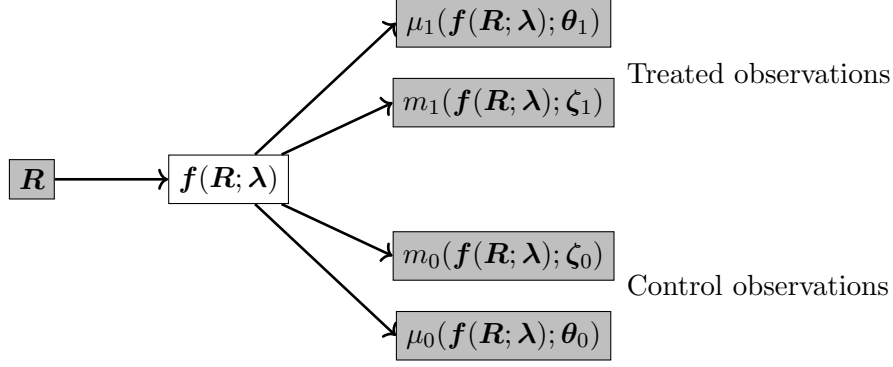


Figure 4: Diagram Illustrating the Proposed Model Architecture with the Instrumental Variable. The proposed model takes an internal representation of a treatment object \mathbf{R}_i as an input, and finds a deconfounder $\mathbf{f}(\mathbf{R}_i)$, which is a lower-dimensional representation of \mathbf{R}_i , and then use it to predict the conditional expectations of the outcome $\mu_t(\mathbf{f}(\mathbf{R}_i)) := \mathbb{E}[Y_i | T_i = t, \mathbf{f}(\mathbf{R}_i)]$ and the perceived treatment feature $m_t(\mathbf{f}(\mathbf{R}_i)) := \mathbb{E}[\tilde{T}_i | T_i = t, \mathbf{f}(\mathbf{R}_i)]$ under each treatment arm t .

of the perceived treatment feature given the treatment feature and deconfounder,

$$m_t(\mathbf{f}(\mathbf{R}_i)) := \mathbb{E}[\tilde{T}_i | T_i = t, \mathbf{f}(\mathbf{R}_i)],$$

for $t \in \{0, 1\}$. Figure 4 presents the proposed neural network architecture that extends the diagram shown in Figure 2 to the instrumental variable setting. The loss function is given by,

$$\{\hat{\lambda}, \hat{\theta}, \hat{\zeta}\} = \underset{\lambda, \theta, \zeta}{\operatorname{argmin}} \frac{1}{n} \sum_{i=1}^n \left[(Y_i - \mu_{T_i}(\mathbf{f}(\mathbf{R}_i); \lambda); \theta_{T_i}))^2 + (\tilde{T}_i - m_{T_i}(\mathbf{f}(\mathbf{R}_i); \lambda); \zeta_{T_i}))^2 \right] \quad (7)$$

Given this neural network architecture, we again use the DML framework for estimation and inference. The exact estimation procedure is described here for completeness.

1. Randomly partition the data into K folds of equal size where the size of each fold is $n = N/K$. The observation index is denoted by $I(i) \in \{1, \dots, K\}$ where $I(i) = k$ implies that the i th observation belongs to the k th fold.
2. For each fold $k \in \{1, \dots, K\}$, use observations with $I(i) \neq k$ as training data:
 - (a) split the training data into two folds, $I_1^{(-k)}$ and $I_2^{(-k)}$
 - (b) obtain estimates of deconfounder and the conditional outcome function on the first fold, denoted by $\hat{\mathbf{f}}^{(-k)}(\{\mathbf{R}_i\}_{i \in I_1^{(-k)}}) := \mathbf{f}(\{\mathbf{R}_i\}_{i \in I_1^{(-k)}}; \hat{\lambda}^{(-k)})$ and $\hat{\mu}_t^{(-k)} := \mu_t(\hat{\mathbf{f}}(\{\mathbf{R}_i\}_{i \in I_1^{(-k)}}; \lambda^{(-k)}); \hat{\theta}^{(-k)})$ and that of the perceived treatment feature $\hat{m}_t^{(-k)}(\{\mathbf{R}_i\}_{i \in I_1^{(-k)}}) := m_t(\mathbf{f}(\{\mathbf{R}_i\}_{i \in I_1^{(-k)}}; \hat{\lambda}^{(-k)}); \hat{\zeta}^{(-k)})$ by solving the optimization problem given in Equation (7), and
 - (c) obtain an estimate of the propensity score given the estimated deconfounder on the second fold, denoted by $\hat{\pi}^{(-k)}(\hat{\mathbf{f}}^{(-k)}(\{\mathbf{R}_i\}_{i \in I_2^{(-k)}})) := \hat{\pi}^{(-k)}(\mathbf{f}(\{\mathbf{R}_i\}_{i \in I_2^{(-k)}}; \hat{\lambda}^{(-k)}))$.
3. Compute an LATE estimate $\hat{\beta}$ as a solution to:

$$\frac{1}{nK} \sum_{k=1}^K \sum_{i: I(i)=k} \psi(\tilde{\mathcal{D}}_i; \hat{\beta}, \hat{\mathbf{f}}^{(-k)}, \hat{\mu}_1^{(-k)}, \hat{\mu}_0^{(-k)}, \hat{m}_1^{(-k)}, \hat{m}_0^{(-k)}, \hat{\pi}^{(-k)}) = 0,$$

where $\tilde{\mathcal{D}}_i := \{Y_i, \tilde{T}_i, T_i, \mathbf{R}_i\}$ and

$$\begin{aligned} & \phi(\tilde{\mathcal{D}}_i; \beta, \mathbf{f}, \mu_1, \mu_0, m_1, m_0, \pi) \\ = & \frac{T_i\{Y_i - \mu_1(\mathbf{f}(\mathbf{R}_i))\}}{\pi(\mathbf{f}(\mathbf{R}_i))} - \frac{(1 - T_i)\{Y_i - \mu_0(\mathbf{f}(\mathbf{R}_i))\}}{1 - \pi(\mathbf{f}(\mathbf{R}_i))} + \mu_1(\mathbf{f}(\mathbf{R}_i)) - \mu_0(\mathbf{f}(\mathbf{R}_i)) \\ & - \left[\frac{T_i\{\tilde{T}_i - m_1(\mathbf{f}(\mathbf{R}_i))\}}{\pi(\mathbf{f}(\mathbf{R}_i))} - \frac{(1 - T_i)\{\tilde{T}_i - m_0(\mathbf{f}(\mathbf{R}_i))\}}{1 - \pi(\mathbf{f}(\mathbf{R}_i))} + m_1(\mathbf{f}(\mathbf{R}_i)) - m_0(\mathbf{f}(\mathbf{R}_i)) \right] \cdot \beta. \end{aligned}$$

Similar to the ATE case, we can establish the asymptotic property of this estimator. We first lay out a set of additional regularity conditions required beyond Assumption 7.

ASSUMPTION 11 (ADDITIONAL REGULARITY CONDITIONS) *Let c_1, c_2 , and $q > 2$ be positive constants and δ_n be a sequence of positive constants approaching zero as the sample size n increases. Then, the following conditions hold:*

(a) *(Primitive condition)*

$$\mathbb{E} \left[\left| (Y_i - \mu_{T_i}(\mathbf{f}(\mathbf{R}_i))) - \beta \cdot (\tilde{T}_i - m_{T_i}(\mathbf{f}(\mathbf{R}_i))) \right|^2 \right]^{1/2} \geq c_2$$

(b) *(Perceived treatment model estimation)*

$$\begin{aligned} \mathbb{E}[m_1(\mathbf{f}(\mathbf{R}_i)) - m_0(\mathbf{f}(\mathbf{R}_i))] & \geq c_2, \quad \mathbb{E}[|\hat{m}_{T_i}(\hat{\mathbf{f}}(\mathbf{R}_i)) - m_{T_i}(\mathbf{f}(\mathbf{R}_i))|^q]^{1/q} \leq c_1, \\ \mathbb{E}[|\hat{m}_{T_i}(\hat{\mathbf{f}}(\mathbf{R}_i)) - m_{T_i}(\mathbf{f}(\mathbf{R}_i))|^2]^{1/2} & \leq \delta_n n^{-1/4}. \end{aligned}$$

Together with Assumption 7, these regularity conditions are essentially equivalent to the assumptions required for DML inference on LATE (Chernozhukov et al., 2018).

Under the above assumptions, the asymptotic normality of the proposed estimator can be established.

THEOREM 4 (ASYMPTOTIC NORMALITY OF INSTRUMENT VARIABLE ESTIMATOR) *Under Assumptions 1–4, 6–11, the estimator $\hat{\beta}$ obtained from the influence function ϕ satisfies asymptotic normality:*

$$\frac{\sqrt{n}(\hat{\beta} - \beta)}{\sigma} \xrightarrow{d} \mathcal{N}(0, 1)$$

where $\sigma^2 = \mathbb{E}[\phi(\tilde{\mathcal{D}}_i; \beta, \mathbf{f}, \mu_1, \mu_0, m_1, m_0, \pi)^2] / \mathbb{E}[\gamma_1(\mathbf{f}(\mathbf{R}_i)) - \gamma_0(\mathbf{f}(\mathbf{R}_i))]^2$.

Proof is omitted given that, like Theorem 2, the result follows immediately from the application of DML theory (Chernozhukov et al., 2018).

5 Simulation Studies

We conduct simulation studies to evaluate the empirical performance of our proposed estimator and compare it to the existing estimators. We use the candidate profile experiment introduced in Section 2 to make the simulation setup realistic.

5.1 Simulation setup

We first generate candidate biographies using an open source LLM, Llama3–8B, that is fine-tuned for instruction-based prompt generations with 8 billion parameters (Touvron et al., 2023). We ask the model to create a biography of politicians under a hypothetical name using the system-level and user-level prompts shown in Table 2. We create hypothetical names by randomly drawing a surname and a first/middle name with replacement from the original corpus of Fong and Grimmer (2016). The total number of biographies in our sample is 4,000.

After generating candidate biographies, we label them based on treatment and confounding features of interest. We consider two scenarios: the first is designed to adhere to the separability assumption (Assumption 5), while the second is likely to violate it. We focus on the separability assumption because it is the key identifying assumption of the proposed methodology.

For the first scenario, we use a candidate’s military background as the treatment variable. A biography is assigned to the treatment group if it contains at least one of the following keywords: “military,” “war,” “veteran,” or “army.” For confounding features, we first consider a combined topic of politics and education, denoted as $h_1(\mathbf{X}_i)$ where h_1 is a complex function of treatment object. That is, we employ a widely-used embedding-based topic model, BERTopic (Grootendorst, 2022), and then assign $h_1(\mathbf{X}_i) = 1$ if a generated biography is classified to a topic whose representative words include “young,” “student,” “college,” “elected,” “senator,” “political,” “graduating,” “education,” and “congressional.” As the second confounding feature, denoted by $h_2(\mathbf{X}_i)$, we use the sentiment analysis module available in the Python TextBlob package, which yields a continuous sentiment polarity score ranging from -1 to 1 . Since the treatment feature is based on a set of specific keywords that are quite different from the confounding features, the separability assumption is likely to be satisfied under this scenario.

For the second scenario, we use two overlapping topics to define the treatment and confounding features so that the separability assumption is likely to be violated. We again use topics obtained from BERTopic, and assign $T_i = 1$ if a generated biography is classified to a topic whose representative words include “college,” “political,” “elected,” “politics,” “student,” “senator,” “education,” “legislative”. For the confounding concept, we set $h_1(\mathbf{X}_i) = 1$ if a biography is assigned to a topic whose representative words include “college,” “political,” “senator,” “politics,” “elected,” “student,” “career.” Thus, although the treatment and confounding concepts are coded based on two different topics, they share many representative words, making it likely for the separability assumption to be violated.

Finally, we use the following linear model with an interaction term to generate the outcome variable,

$$Y_i = \alpha_1 T_i + \alpha_2 T_i h_1(\mathbf{X}_i) - \alpha_3 h_1(\mathbf{X}_i) - \alpha_4 h_2(\mathbf{X}_i) + \epsilon_i,$$

where ϵ_i is the standard normal random variable. Although the model may appear to be a relatively simple function of the treatment and confounding features, these variables themselves are complex functions of texts. Thus, inferring the ATE is not straightforward because it requires learning an accurate representation of confounding features.

To evaluate the performance of each estimator, we assume that researchers do not have access to the confounding features, $h_1(\mathbf{X}_i)$ and $h_2(\mathbf{X}_i)$. We wish to infer the ATE, which is given by $\tau = \alpha_1 + \alpha_2 \mathbb{E}[h_1(\mathbf{X}_i)]$ where we set $\alpha_1 = \alpha_2 = 10$ throughout the simulations. We consider the three scenarios: (1) weak confounding $\alpha_3 = \alpha_4 = 50$, (2) moderate confounding $\alpha_3 = \alpha_4 = 100$, (3) strong confounding $\alpha_3 = \alpha_4 = 1000$. Given the computational cost, our evaluation is conditional on a single set of generated biographies and its associated treatment and confounding variables. Therefore, $\mathbb{E}[h_1(\mathbf{X}_i)]$ is set to its sample mean, and randomness comes only from the error term of the outcome model ϵ_i .

5.2 Estimators to be compared

Once Llama3 generates all biographies, we extract an internal representation of each biography from the last hidden layer whose dimension is $4096 \times$ the number of tokens contained in the biography. For text reuse, we simply ask the LLM to repeat each of the generated texts. To compute the proposed estimator, we follow the discussion presented in Section 3.4 and use the representation of the last token, yielding a 4096 dimensional vector of internal representation for each candidate biography.

In our neural network architecture, we use one linear layer for the deconfounder $\mathbf{f}(\mathbf{R}_i)$ whose output dimension is 2048. Similarly, we utilize two consecutive linear layers for the potential outcome models whose output dimensions are 500 and 1. We apply ReLU as an activation function between each layer, and also use a dropout rate of 0.15 to prevent overfitting. We select the neural network architecture, including dropout rates, layer depth, and dimension of each layer, based on additional hyperparameter tuning under the weak confounding setting. While we do not conduct hyperparameter tuning for each setting separately, we find that minor changes in these hyperparameters do not significantly affect the value of the loss function.

We use 40% of our data as a training set, 10% as a validation set, and the remaining 50% is used to perform the downstream causal effect estimation. For optimization, we set the batch size to 32 and train the model for 500 epochs, and use early stopping to prevent overfitting. Specifically, we stop training if the estimated loss does not improve for more than 15 epochs. Since the performance of the methodology can depend on the choice of hyperparameters, especially learning rates, we select the learning rates using an automated hyperparameter tuning package `Optuna`. We do not include the size of the deconfounder as a hyperparameter to be tuned because tuning it for the BERT-based methods is computationally too expensive. We also do not observe any substantial difference in performance when varying the dimensions of the deconfounder for the proposed methodology. Once the outcome model is fitted, we estimate the propensity score via a random forest classifier with the estimated deconfounder, using the `scikit-learn` library.

We evaluate the performance of the proposed estimator in comparison to the following three estimators. First, to establish a baseline, we use the difference-in-means estimator, which does not make any adjustment for confounding. Second, we implement the two existing approaches that estimate vectorized representation of texts using the BERT embedding $\mathbf{b}(\cdot)$; Pryzant et al. (2021) estimates nuisance functions with TarNet and calculates the causal effect using a T-learner, while Gui and Veitch (2023) uses the same outcome models as Pryzant et al. (2021) but applies DML with the estimated propensity score. Importantly, both of these approaches are based on the following loss function,

$$\frac{\lambda}{n} \sum_{i=1}^n \{Y_i - Q_{T_i}(\mathbf{b}(\mathbf{X}_i))\}^2 - \frac{\alpha}{n} \sum_{i=1}^n \left\{ T_i \log g(\mathbf{b}(\mathbf{X}_i)) + (1 - T_i) \log[1 - g(\mathbf{b}(\mathbf{X}_i))] \right\} + \frac{1}{n} \sum_{i=1}^n B(\mathbf{b}_{\text{full}}(\mathbf{X}_i)) \quad (8)$$

where $Q_t(\cdot)$ is the outcome model under $T_i = t$, $g(\cdot)$ is the treatment prediction, $B(\cdot)$ is the original BERT masked language loss for estimating vector representations of texts from the embedding $\mathbf{b}(\cdot)$, and $\alpha, \lambda \in \mathbb{R}$ are the hyperparameters (Veitch et al., 2020). Only the first token’s vector representation $\mathbf{b}(\cdot)$ is used for outcome and treatment predictions because it is the special token called [CLS] token that contains the entire semantic information. On the other hand, for the masked language loss, the entire embedding $\mathbf{b}_{\text{full}}(\cdot)$ is used. The loss function given in Equation (8) differs from our loss function (Equation (3)) in that in addition to the outcome model, it optimizes the representation learning from texts and the treatment prediction.

After estimating the nuisance functions, Gui and Veitch (2023) proposes to estimate the propen-

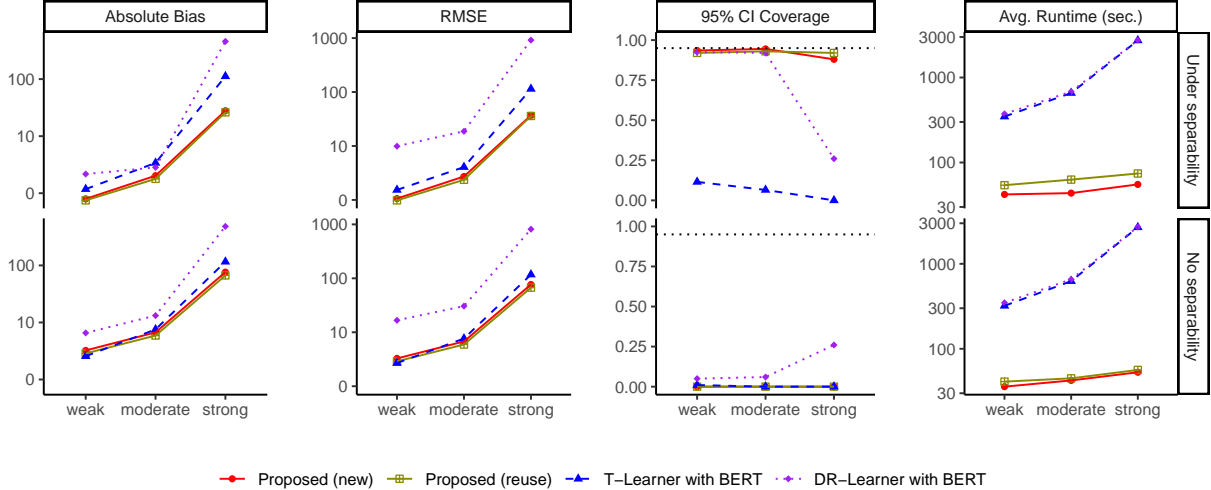


Figure 5: Performance of Five Estimators under Different Confounding Scenarios (Weak, Moderate, and Strong) under Separability (top row) and No Separability (bottom row). A red solid line represents the proposed methodology for the new texts, while a dark yellow solid line represents that for the regenerated texts (text reuse). For comparison, we also include T-learner with BERT (blue) and DR-learner with BERT (purple). The black horizontal dotted line in the 95% Confidence Interval (CI) Coverage panel represents the nominal coverage of 95%.

sity score model by treating $Q_1(\mathbf{b}(\mathbf{X}_i))$ and $Q_0(\mathbf{b}(\mathbf{X}_i))$ as covariates, i.e., $\Pr(T_i = 1 \mid \mathbf{X}_i) = g(Q_1(\mathbf{b}(\mathbf{X}_i)), Q_0(\mathbf{b}(\mathbf{X}_i)))$. For propensity score estimation, we use a Gaussian Process, as recommended by Gui and Veitch (2023). We truncate the extreme values of the estimated propensity scores at 0.01 and 0.99 for DR-learner with BERT though such truncation is not necessary for the proposed methodology. For DR-learner with BERT, this truncation occurs even when the separability assumption is satisfied (roughly 5% of time for weak and moderate confounding, and 45% for strong confounding). Without truncation, the bias and RMSE are not computable for these methods. Finally, we follow the default hyperparameter in the original code of the authors and set $\alpha = \lambda = 1$ while tuning the other hyperparameters regarding the learning rate in the same way as done for our estimator.

5.3 Simulation results

Figure 5 graphically displays the results of our simulation studies while Appendix S2 reports the corresponding numerical results. Our results are based on 200 Monte Carlo trials. We choose this relatively small number of trials because, unlike the proposed estimator, the BERT-based estimators are computationally intensive. Appendix S2 also presents the simulation results based on 1,000 Monte Carlo trials for the proposed estimator alone. As expected, the results are qualitatively similar to those presented in this section.

We find that when the separability assumption holds (top row), our proposed estimators (red line for new texts and dark yellow for text reuse) exhibit smaller bias and RMSE compared to all the other estimators, with the 95% confidence interval coverage closely matching the nominal rate. The performance differences are particularly striking in the strong confounding setting, where DR-learner with BERT (purple) performs poorly, unlike the weak and moderate confounding scenarios. Additionally, T-learner with BERT (blue) has severe undercoverage across all simulation scenarios, whereas the confidence interval of DR-learner with BERT breaks down only under the strong

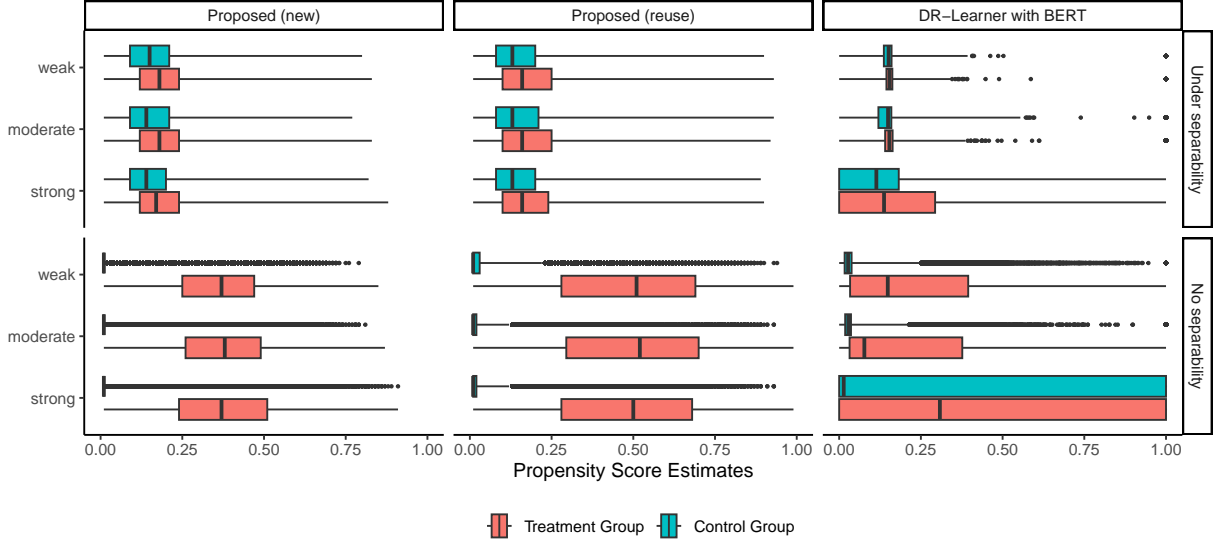


Figure 6: Distribution of the Estimated Propensity Scores for the Treatment (red) and Control (blue) Groups. We present the results for the proposed estimator (new texts in the left panels, and text reuse in the middle panels), and DR-learner with BERT (right) under the separability assumption (top) and no separability (bottom). Under each scenario, we present the results based on three different strengths of confounding; weak, moderate, and strong. For the proposed methodologies, the estimated propensity scores are distributed similarly across different confounding scenarios under the separability assumption. In contrast, for DR-learner with BERT, the distribution is heavily skewed right under the strong confounding scenario. When the separability assumption is violated, both methods have extremely small estimated propensity scores for the control group.

confounding scenario. Lastly, our estimators are more than ten times as computationally efficient as BERT-based estimators, when measured in terms of the average runtime.

In contrast, when the separability assumption is violated (bottom row), all estimators, including ours, perform poorly. Under this setting, both bias and RMSE grow as the strength of confounding increases. As a result, the coverage of confidence intervals no longer approximates the nominal coverage rate even for the proposed estimator.

We further examine the difference in performance between the proposed estimator and DR-learner with BERT. Figure 6 shows the distribution of estimated propensity scores without truncation (recall that truncation is not needed for the proposed methodology). For the proposed methodology, when the separability assumption is met (top and middle left panel), the distribution of estimated propensity scores is relatively symmetric regardless of the strength of confounding and is similar between the treatment and control groups. Indeed, most observations have estimated propensity scores that are away from zero. This explains why the proposed estimator performs well under this scenario.

On the other hand, when the separability assumption is violated (bottom left and middle panels), the estimated propensity scores for the control group are heavily skewed to the right and are close to zero, indicating that the overlap assumption is violated. This suggests that visualizing propensity scores can help diagnose the potential violation of the separability assumption for our proposed method, which leads to complete entanglement between the treatment and confounding features and causes the deconfounder to perfectly predict the treatment assignment. In contrast,

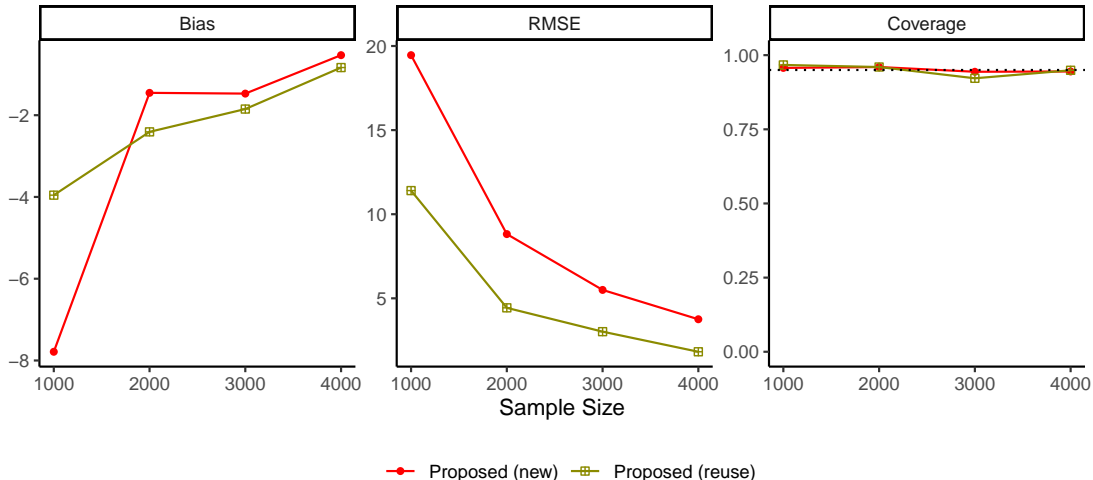


Figure 7: Performance of the Proposed Estimator on the created texts (red) and the reused texts (blue) for Different Sample Size based on 1000 Monte Carlo trials. The data generating process is no interaction setting ($\alpha_1 = 10, \alpha_2 = 0, \alpha_3 = \alpha_4 = 100$). The black dotted line in the coverage panel represents the nominal coverage of 95%.

DR-learner with BERT yields a wide range of estimated propensity scores under the strong confounding settings (top right panel), in which the estimator performs poorly. This pattern is observed even when the separability assumption is violated (bottom right panel). The finding implies that, unlike the proposed estimator, extreme values of estimated propensity scores may not serve as a reliable diagnostic for DR-learner with BERT.

Finally, we examine the performance of the proposed estimator for new texts and text reuse as we vary the sample size from 1,000 to 4,000 under the assumption of separability. For this simulation, we use the moderate confounding setting without interaction term ($\alpha_1 = 10, \alpha_2 = 0, \alpha_3 = \alpha_4 = 100$) so that the true ATE stays identical across sample sizes. We conduct 1,000 Monte Carlo trials as we focus only on the proposed estimator, which is computationally efficient. Figure 7 presents bias, RMSE, and coverage for each sample size. As expected, both bias and RMSE become smaller as the sample size increases. We also find that the empirical coverage of the 95% confidence intervals stays close to the nominal coverage even when the sample size is as small as 1000. Interestingly, while bias is similar between new texts and text reuse, RMSE (hence variance) is substantially smaller for text reuse. In sum, the proposed methodology performs well across different sample sizes so long as the separability assumption is satisfied.

6 Empirical Analysis

Finally, we apply the proposed methodology to human responses (rather than simulated data) from the candidate profile experiment of Fong and Grimmer (2016) using pre-defined treatment coding. In the original experiment, the authors scraped 1,246 Congressional candidate biographies from Wikipedia, randomly assigned up to four biographies to 1,886 survey participants, and asked respondents how they felt about each candidate using the standard feeling thermometer ranging from 0 to 100, where a higher value indicates a more favorable evaluation. The total number of observations we analyze is 5,291 after dropping some observations with empty texts.

While Fong and Grimmer (2016) use a Bayesian topic model to discover treatments from the data, we instead use the pre-defined treatment coding. As in the simulation studies, we use a

Methods	ATE Estimates	95% Confidence Interval	Runtime (sec.)
Proposed method (reuse)	5.462	[2.790, 8.135]	28.9
T-learner with BERT	-2.557	[-2.608, -2.505]	6139.7
DR-learner with BERT	-67.777	[-109.967, -25.587]	6210.3

Table 3: The Estimated Average Treatment Effect (ATE) for the Candidate Profile Experiment.

candidate’s military background as the treatment variable by assigning a biography to the treatment group if it contains at least one of the following keywords: “military,” “war,” “veteran,” and “army.” According to this coding rule, only about seven percent of the biographies (362 out of 5,291) are in the treatment group.

For causal effect estimation, we take the text reuse approach by regenerating each biography using Llama3-8B. We then apply the proposed methodology by following the procedure described in Section 3 with two-fold cross fitting. For comparison, as done in our simulation studies, we also apply the two existing BERT-based methods — Pryzant et al. (2021) (T-learner with BERT) and Gui and Veitch (2023) (DR-learner with BERT).

Table 3 presents the results. The analysis based on the proposed methodology implies that military experience has a positive effect and it is statistically significant. This echoes with the finding of Fong and Grimmer (2016), who also found that the topic corresponding to military experience has a statistically significant positive association with a higher feeling thermometer score. Moreover, both T-learner and DR-learner with BERT yield negative and statistically significant point estimates. This is at least in part due to the violation of positivity. Indeed, for the BERT-based estimators, all 5291 observations have estimated propensities scores outside of the range of [0.01, 0.99]. Lastly, as observed in our simulation studies, the runtime for our proposed estimator is more than 200 times shorter than that of the other two BERT-based estimators.

7 Concluding Remarks

In this paper, we demonstrate that the use of generative AI can significantly enhance the validity of causal inference with unstructured treatments, such as texts and images. The proposed methodology leverages generative AI to both efficiently produce a variety of textual treatments and precisely control confounding bias. By utilizing the true vector representation of generated texts, we avoid need to estimate such representation from texts as done in the previous methods, leading to more efficient and robust causal effect estimation. We formalize the conditions required for nonparametric identification, showing that the separability of treatment and confounding features plays an essential role. We also develop an estimation strategy based on a neural network architecture that mitigate the risk of positivity violation, which commonly occurs to the existing methods. Lastly, we extend the proposed methodology to the settings of perceived treatments, using an instrumental variables approach. Our simulation study shows that the proposed estimator outperforms the existing methods, which estimate the representation of textual treatments from texts themselves.

Although we have focused on texts as treatments in this paper, our proposed approach can be extended to other types of unstructured data, such as images and videos. For images, we expect the proposed methodology to work as it is so long as the dimensionality of internal representation is relatively low. If the dimensionality is high, architectures like convolutional neural networks may be needed to effectively reduce input dimensions. For videos, both treatment and confounding features are likely to exhibit complex relationships due to the combination of audio and images with the additional temporal dimension. Thus, the methodology described here is not readily applicable.

Future work should consider how to leverage the internal representation of videos obtained from generative AI.

References

- Ahrens, M., Ashwin, J., Calliess, J.-P., and Nguyen, V. (2021). Bayesian Topic Regression for Causal Inference. arXiv:2109.05317 [cs, stat].
- Akiba, T., Sano, S., Yanase, T., Ohta, T., and Koyama, M. (2019). Optuna: A Next-generation Hyperparameter Optimization Framework. In *Proceedings of the 25th ACM SIGKDD International Conference on Knowledge Discovery & Data Mining*, KDD '19, pages 2623–2631, New York, NY, USA. Association for Computing Machinery.
- Aronow, P. M., Baron, J., and Pinson, L. (2019). A Note on Dropping Experimental Subjects who Fail a Manipulation Check. *Political Analysis*, 27(4):572–589. Publisher: Cambridge University Press.
- Bisbee, J., Clinton, J. D., Dorff, C., Kenkel, B., and Larson, J. M. (2024). Synthetic Replacements for Human Survey Data? The Perils of Large Language Models. *Political Analysis*, pages 1–16.
- Blackwell, M., Brown, J. R., Hill, S., Imai, K., and Yamamoto, T. (2023). Priming bias versus post-treatment bias in experimental designs. arXiv:2306.01211 [stat].
- Campbell, R. and Cowley, P. (2014). What Voters Want: Reactions to Candidate Characteristics in a Survey Experiment. *Political Studies*, 62(4):745–765. Publisher: SAGE Publications Ltd.
- Chernozhukov, V., Chetverikov, D., Demirer, M., Duflo, E., Hansen, C., Newey, W., and Robins, J. (2018). Double/debiased machine learning for treatment and structural parameters. *The Econometrics Journal*, 21(1):C1–C68.
- Chowdhery, A., Narang, S., Devlin, J., Bosma, M., Mishra, G., Roberts, A., Barham, P., Chung, H. W., Sutton, C., Gehrmann, S., Schuh, P., Shi, K., Tsvyashchenko, S., Maynez, J., Rao, A., Barnes, P., Tay, Y., Shazeer, N., Prabhakaran, V., Reif, E., Du, N., Hutchinson, B., Pope, R., Bradbury, J., Austin, J., Isard, M., Gur-Ari, G., Yin, P., Duke, T., Levskaya, A., Ghemawat, S., Dev, S., Michalewski, H., Garcia, X., Misra, V., Robinson, K., Fedus, L., Zhou, D., Ippolito, D., Luan, D., Lim, H., Zoph, B., Spiridonov, A., Sepassi, R., Dohan, D., Agrawal, S., Omernick, M., Dai, A. M., Pillai, T. S., Pellat, M., Lewkowycz, A., Moreira, E., Child, R., Polozov, O., Lee, K., Zhou, Z., Wang, X., Saeta, B., Diaz, M., Firat, O., Catasta, M., Wei, J., Meier-Hellstern, K., Eck, D., Dean, J., Petrov, S., and Fiedel, N. (2022). PaLM: Scaling Language Modeling with Pathways. arXiv:2204.02311 [cs].
- Daoud, A., Jerzak, C. T., and Johansson, R. (2022). Conceptualizing Treatment Leakage in Text-based Causal Inference. arXiv:2205.00465 [cs].
- Dawid, A. P. (1979). Conditional Independence in Statistical Theory. *Journal of the Royal Statistical Society. Series B (Methodological)*, 41(1):1–31. Publisher: [Royal Statistical Society, Wiley].
- Devlin, J., Chang, M.-W., Lee, K., and Toutanova, K. (2019). BERT: Pre-training of Deep Bidirectional Transformers for Language Understanding. arXiv:1810.04805 [cs].
- Egami, N., Fong, C. J., Grimmer, J., Roberts, M. E., and Stewart, B. M. (2022). How to make causal inferences using texts. *Science Advances*, 8(42):eabg2652. Publisher: American Association for the Advancement of Science.

- Egami, N. and Hartman, E. (2023). Elements of external validity: Framework, design, and analysis. *American Political Science Review*, 117(3):1070–1088.
- Egami, N. and Imai, K. (2019). Causal Interaction in Factorial Experiments: Application to Conjoint Analysis. *Journal of the American Statistical Association*, 114(526):529–540.
- Farrell, M. H., Liang, T., and Misra, S. (2021). Deep Neural Networks for Estimation and Inference. *Econometrica*, 89(1):181–213. [eprint: https://onlinelibrary.wiley.com/doi/pdf/10.3982/ECTA16901](https://onlinelibrary.wiley.com/doi/pdf/10.3982/ECTA16901).
- Feder, A., Keith, K. A., Manzoor, E., Pryzant, R., Sridhar, D., Wood-Doughty, Z., Eisenstein, J., Grimmer, J., Reichart, R., Roberts, M. E., Stewart, B. M., Veitch, V., and Yang, D. (2022). Causal Inference in Natural Language Processing: Estimation, Prediction, Interpretation and Beyond. arXiv:2109.00725 [cs].
- Fong, C. and Grimmer, J. (2016). Discovery of Treatments from Text Corpora. In *Proceedings of the 54th Annual Meeting of the Association for Computational Linguistics (Volume 1: Long Papers)*, pages 1600–1609, Berlin, Germany. Association for Computational Linguistics.
- Fong, C. and Grimmer, J. (2023). Causal Inference with Latent Treatments. *American Journal of Political Science*, 67(2):374–389. [eprint: https://onlinelibrary.wiley.com/doi/pdf/10.1111/ajps.12649](https://onlinelibrary.wiley.com/doi/pdf/10.1111/ajps.12649).
- Gouk, H., Frank, E., Pfahringer, B., and Cree, M. J. (2021). Regularisation of neural networks by enforcing lipschitz continuity. *Machine Learning*, 110:393–416.
- Grootendorst, M. (2022). BERTopic: Neural topic modeling with a class-based TF-IDF procedure. arXiv:2203.05794 [cs].
- Gui, L. and Veitch, V. (2023). Causal Estimation for Text Data with (Apparent) Overlap Violations. arXiv:2210.00079 [cs, stat].
- Guo, B., Gong, Y., Shen, Y., Han, S., Huang, H., Duan, N., and Chen, W. (2022). GENIUS: Sketch-based Language Model Pre-training via Extreme and Selective Masking for Text Generation and Augmentation. arXiv:2211.10330 [cs].
- Hainmueller, J., Hopkins, D. J., and Yamamoto, T. (2014). Causal Inference in Conjoint Analysis: Understanding Multidimensional Choices via Stated Preference Experiments. *Political Analysis*, 22(1):1–30. Publisher: Cambridge University Press.
- Ho, J., Jain, A., and Abbeel, P. (2020). Denoising Diffusion Probabilistic Models. arXiv:2006.11239 [cs, stat].
- Hu, Z. and Li, L. E. (2021). A Causal Lens for Controllable Text Generation. In *Advances in Neural Information Processing Systems*, volume 34, pages 24941–24955. Curran Associates, Inc.
- Imai, K. and Jiang, Z. (2019). Comment: The challenges of multiple causes. *Journal of the American Statistical Association*, 114(528):1605–1610.
- Imai, K. and Van Dyk, D. A. (2004). Causal Inference With General Treatment Regimes: Generalizing the Propensity Score. *Journal of the American Statistical Association*, 99(467):854–866.

- Imbens, G. W. and Angrist, J. D. (1994). Identification and Estimation of Local Average Treatment Effects. *Econometrica*, 62(2):467–475. Publisher: [Wiley, Econometric Society].
- Jerzak, C. T., Johansson, F., and Daoud, A. (2023a). Integrating Earth Observation Data into Causal Inference: Challenges and Opportunities. arXiv:2301.12985 [cs, stat].
- Jerzak, C. T., Johansson, F. D., and Daoud, A. (2023b). Image-based Treatment Effect Heterogeneity. In *Proceedings of the Second Conference on Causal Learning and Reasoning*, pages 531–552. PMLR. ISSN: 2640-3498.
- Jiang, A. Q., Sablayrolles, A., Mensch, A., Bamford, C., Chaplot, D. S., Casas, D. d. l., Bressand, F., Lengyel, G., Lample, G., Saulnier, L., Lavaud, L. R., Lachaux, M.-A., Stock, P., Scao, T. L., Lavril, T., Wang, T., Lacroix, T., and Sayed, W. E. (2023). Mistral 7B. arXiv:2310.06825.
- Kasneci, E., Sessler, K., Küchemann, S., Bannert, M., Dementieva, D., Fischer, F., Gasser, U., Groh, G., Günemann, S., Hüllermeier, E., Krusche, S., Kutyniok, G., Michaeli, T., Nerdel, C., Pfeffer, J., Poquet, O., Sailer, M., Schmidt, A., Seidel, T., Stadler, M., Weller, J., Kuhn, J., and Kasneci, G. (2023). Chatgpt for good? on opportunities and challenges of large language models for education. *Learning and Individual Differences*, 103:102274.
- Keith, K. A., Jensen, D., and O’Connor, B. (2020). Text and Causal Inference: A Review of Using Text to Remove Confounding from Causal Estimates. arXiv:2005.00649 [cs].
- Keskar, N. S., McCann, B., Varshney, L. R., Xiong, C., and Socher, R. (2019). CTRL: A Conditional Transformer Language Model for Controllable Generation. arXiv:1909.05858 [cs].
- Kirkland, P. A. and Coppock, A. (2018). Candidate Choice Without Party Labels:. *Political Behavior*, 40(3):571–591.
- Klaassen, S., Teichert-Kluge, J., Bach, P., Chernozhukov, V., Spindler, M., and Vijaykumar, S. (2024). DoubleMLDeep: Estimation of Causal Effects with Multimodal Data. arXiv:2402.01785 [cs, econ, stat].
- Klar, S., Leeper, T., and Robison, J. (2020). Studying Identities with Experiments: Weighing the Risk of Posttreatment Bias Against Priming Effects. *Journal of Experimental Political Science*, 7(1):56–60.
- Kshetri, N., Dwivedi, Y. K., Davenport, T. H., and Panteli, N. (2024). Generative artificial intelligence in marketing: Applications, opportunities, challenges, and research agenda. *International Journal of Information Management*, 75:102716.
- Lewis, M., Liu, Y., Goyal, N., Ghazvininejad, M., Mohamed, A., Levy, O., Stoyanov, V., and Zettlemoyer, L. (2020). BART: Denoising Sequence-to-Sequence Pre-training for Natural Language Generation, Translation, and Comprehension. In Jurafsky, D., Chai, J., Schluter, N., and Tetreault, J., editors, *Proceedings of the 58th Annual Meeting of the Association for Computational Linguistics*, pages 7871–7880, Online. Association for Computational Linguistics.
- Ludwig, J. and Mullainathan, S. (2024). Machine Learning as a Tool for Hypothesis Generation*. *The Quarterly Journal of Economics*, 139(2):751–827.
- Montgomery, J. M., Nyhan, B., and Torres, M. (2018). How Conditioning on Posttreatment Variables Can Ruin Your Experiment and What to Do about It. *American Journal of Political Science*, 62(3):760–775. _eprint: <https://onlinelibrary.wiley.com/doi/pdf/10.1111/ajps.12357>.

- Mozer, R., Kaufman, A. R., Celi, L. A., and Miratrix, L. (2024). Leveraging text data for causal inference using electronic health records. arXiv:2307.03687 [cs, stat].
- Mozer, R., Miratrix, L., Kaufman, A. R., and Anastasopoulos, L. J. (2020). Matching with Text Data: An Experimental Evaluation of Methods for Matching Documents and of Measuring Match Quality. *Political Analysis*, 28(4):445–468. Publisher: Cambridge University Press.
- Ni, J., Ábrego, G. H., Constant, N., Ma, J., Hall, K. B., Cer, D., and Yang, Y. (2021). Sentence-T5: Scalable Sentence Encoders from Pre-trained Text-to-Text Models. arXiv:2108.08877 [cs].
- Pedersen, R. T., Dahlgaard, J. O., and Citi, M. (2019). Voter reactions to candidate background characteristics depend on candidate policy positions. *Electoral Studies*, 61:102066.
- Pryzant, R., Card, D., Jurafsky, D., Veitch, V., and Sridhar, D. (2021). Causal Effects of Linguistic Properties. arXiv:2010.12919 [cs].
- Radford, A., Narasimhan, K., Salimans, T., and Sutskever, I. (2018). Improving Language Understanding by Generative Pre-Training.
- Raffel, C., Shazeer, N., Roberts, A., Lee, K., Narang, S., Matena, M., Zhou, Y., Li, W., and Liu, P. J. (2023). Exploring the Limits of Transfer Learning with a Unified Text-to-Text Transformer. arXiv:1910.10683 [cs, stat].
- Ramesh, A., Pavlov, M., Goh, G., Gray, S., Voss, C., Radford, A., Chen, M., and Sutskever, I. (2021). Zero-Shot Text-to-Image Generation. In *Proceedings of the 38th International Conference on Machine Learning*, pages 8821–8831. PMLR. ISSN: 2640-3498.
- Roberts, M. E., Stewart, B. M., and Nielsen, R. A. (2020). Adjusting for Confounding with Text Matching. *American Journal of Political Science*, 64(4):887–903. eprint: <https://onlinelibrary.wiley.com/doi/pdf/10.1111/ajps.12526>.
- Rombach, R., Blattmann, A., Lorenz, D., Esser, P., and Ommer, B. (2022). High-Resolution Image Synthesis With Latent Diffusion Models. pages 10684–10695.
- Rubin, D. B. (1990). Comments on “On the application of probability theory to agricultural experiments. Essay on principles. Section 9” by J. Splawa-Neyman translated from the Polish and edited by D. M. Dabrowska and T. P. Speed. *Statistical Science*, 5:472–480.
- Shalit, U., Johansson, F. D., and Sontag, D. (2017). Estimating individual treatment effect: generalization bounds and algorithms. arXiv:1606.03976 [cs, stat].
- Shi, C., Blei, D., and Veitch, V. (2019). Adapting Neural Networks for the Estimation of Treatment Effects. In *Advances in Neural Information Processing Systems*, volume 32. Curran Associates, Inc.
- Shrestha, R. and Xie, B. (2023). Conditional Image Generation with Pretrained Generative Model. arXiv:2312.13253 [cs].
- Song, Y., Sohl-Dickstein, J., Kingma, D. P., Kumar, A., Ermon, S., and Poole, B. (2020). Score-Based Generative Modeling through Stochastic Differential Equations.
- Su, Y., Lan, T., Wang, Y., Yogatama, D., Kong, L., and Collier, N. (2022). A Contrastive Framework for Neural Text Generation. arXiv:2202.06417 [cs].

- Thirunavukarasu, A. J., Ting, D. S. J., Elangovan, K., Gutierrez, L., Tan, T. F., and Ting, D. S. W. (2023). Large language models in medicine. *Nature Medicine*, 29(8):1930–1940.
- Touvron, H., Lavril, T., Izacard, G., Martinet, X., Lachaux, M.-A., Lacroix, T., Rozière, B., Goyal, N., Hambro, E., Azhar, F., Rodriguez, A., Joulin, A., Grave, E., and Lample, G. (2023). LLaMA: Open and Efficient Foundation Language Models. arXiv:2302.13971 [cs].
- van Waarde, H. and Sepulchre, R. (2022). Training lipschitz continuous operators using reproducing kernels. In *Learning for Dynamics and Control Conference*, pages 221–233. PMLR.
- Veitch, V., Sridhar, D., and Blei, D. M. (2020). Adapting Text Embeddings for Causal Inference. arXiv:1905.12741 [cs, stat].
- Wang, Y. and Blei, D. M. (2019). The blessings of multiple causes. *Journal of the American Statistical Association*, 114(528):1574–1596.
- Wang, Y. and Jordan, M. I. (2022). Desiderata for Representation Learning: A Causal Perspective. arXiv:2109.03795 [cs, stat].
- Yang, K. and Klein, D. (2021). FUDGE: Controlled Text Generation With Future Discriminators. In *Proceedings of the 2021 Conference of the North American Chapter of the Association for Computational Linguistics: Human Language Technologies*, pages 3511–3535. arXiv:2104.05218 [cs].
- Ye, H., Zhang, J., Liu, S., Han, X., and Yang, W. (2023). IP-Adapter: Text Compatible Image Prompt Adapter for Text-to-Image Diffusion Models. arXiv:2308.06721 [cs].
- Zhang, S., Roller, S., Goyal, N., Artetxe, M., Chen, M., Chen, S., Dewan, C., Diab, M., Li, X., Lin, X. V., Mihaylov, T., Ott, M., Shleifer, S., Shuster, K., Simig, D., Koura, P. S., Sridhar, A., Wang, T., and Zettlemoyer, L. (2022). OPT: Open Pre-trained Transformer Language Models. arXiv:2205.01068 [cs].
- Zhou, W., Jiang, Y. E., Wilcox, E., Cotterell, R., and Sachan, M. (2023). Controlled Text Generation with Natural Language Instructions. arXiv:2304.14293 [cs].

S1 Proofs

S1.1 Proof of Lemma 1

We use proof by contradiction. Suppose that the overlap condition is not satisfied. That is, there exist $t \in \{0, 1\}$ and $\mathbf{u} \in \mathcal{U}$ such that $\mathbb{P}(T_i = t \mid \mathbf{U}_i = \mathbf{u}) = 0$ or equivalently $\mathbb{P}(T_i = t' \mid \mathbf{U}_i = \mathbf{u}) = 1$ where $t' = 1 - t$. This implies that under Assumptions 3 and 4, there exists a deterministic function \tilde{g} and \mathbf{x} such that $t = \tilde{g}(\mathbf{u}) = \tilde{g} \circ \mathbf{g}_{\mathcal{U}}(\mathbf{x})$. This contradicts Assumption 5. \square

S1.2 Proof of Theorem 1

Under a deep generative model (see Definition 1), the distribution of \mathbf{X}_i only depends on \mathbf{P}_i , and hence we have $Y_i(\mathbf{x}) \perp\!\!\!\perp \mathbf{X}_i \mid \mathbf{P}_i$. Together with Assumption 2, Lemma 4.3 of Dawid (1979) implies $Y_i(\mathbf{x}) \perp\!\!\!\perp \mathbf{X}_i$. Then, under Assumptions 3 and 5, we have:

$$Y_i(t, \mathbf{U}_i) \perp\!\!\!\perp T_i \mid \mathbf{U}_i. \quad (\text{S1})$$

Next, under Assumptions 3, 4, and 6, \mathbf{U}_i is a deterministic function of \mathbf{R}_i such that we can write $\mathbf{U}_i = \mathbf{f}^*(\mathbf{R}_i)$ for some function \mathbf{f}^* . Note that Assumption 5 implies $Y_i \perp\!\!\!\perp \mathbf{R}_i \mid T_i = t, \mathbf{f}^*(\mathbf{R}_i)$. Thus, we have:

$$\begin{aligned} \mathbb{P}(Y_i(t, \mathbf{U}_i) = y) &= \int_{\mathcal{U}} \mathbb{P}(Y_i(t, \mathbf{U}_i) = y \mid \mathbf{U}_i) dF(\mathbf{U}_i) \\ &= \int_{\mathcal{U}} \mathbb{P}(Y_i(t, \mathbf{U}_i) = y \mid T_i = t, \mathbf{U}_i) dF(\mathbf{U}_i) \\ &= \int_{\mathcal{U}} \mathbb{P}(Y_i = y \mid T_i = t, \mathbf{f}^*(\mathbf{R}_i)) dF(\mathbf{f}^*(\mathbf{R}_i)), \\ &= \int_{\mathbb{R}^r} \mathbb{P}(Y_i = y \mid T_i = t, \mathbf{f}^*(\mathbf{R}_i)) dF(\mathbf{R}_i), \end{aligned}$$

where the second equality follows from Equation (S1) and Lemma 1, and the third equality is due to Assumption 1. Finally, suppose there is another function $\mathbf{f}(\mathbf{R}_i)$ which satisfies the conditional independence relation $Y_i \perp\!\!\!\perp \mathbf{R}_i \mid T_i = t, \mathbf{f}(\mathbf{R}_i)$. Then,

$$\begin{aligned} \int_{\mathbb{R}^r} \mathbb{P}(Y_i = y \mid T_i = t, \mathbf{f}(\mathbf{R}_i)) dF(\mathbf{R}_i) &= \int_{\mathbb{R}^r} \mathbb{P}(Y_i = y \mid T_i = t, \mathbf{f}(\mathbf{R}_i), \mathbf{R}_i) dF(\mathbf{R}_i) \\ &= \int_{\mathbb{R}^r} \mathbb{P}(Y_i = y \mid T_i = t, \mathbf{f}^*(\mathbf{R}_i), \mathbf{R}_i) dF(\mathbf{R}_i) \\ &= \int_{\mathbb{R}^r} \mathbb{P}(Y_i = y \mid T_i = t, \mathbf{f}^*(\mathbf{R}_i)) dF(\mathbf{R}_i) \end{aligned}$$

Thus, any function of \mathbf{R}_i that satisfies this conditional independence relation leads to the same identification formula. \square

S1.3 Proof of Theorem 2

Assumptions 7(c)–(d) and the triangle inequality imply,

$$\begin{aligned} \mathbb{E}[|\hat{\pi}(\hat{\mathbf{f}}(\mathbf{R}_i)) - \pi(\mathbf{f}(\mathbf{R}_i))|^q]^{1/q} &= \mathbb{E}[|\{\hat{\pi}(\hat{\mathbf{f}}(\mathbf{R}_i)) - \hat{\pi}(\mathbf{f}(\mathbf{R}_i))\} + \{\hat{\pi}(\mathbf{f}(\mathbf{R}_i)) - \pi(\mathbf{f}(\mathbf{R}_i))\}|^q]^{1/q} \\ &\leq \mathbb{E}[|\hat{\pi}(\hat{\mathbf{f}}(\mathbf{R}_i)) - \hat{\pi}(\mathbf{f}(\mathbf{R}_i))|^q]^{1/q} + c_1 \\ &\leq L \cdot \mathbb{E}\left[\left\|\hat{\mathbf{f}}(\mathbf{R}_i) - \mathbf{f}(\mathbf{R}_i)\right\|^q\right]^{1/q} + c_1 \\ &= (L + 1)c_1 \end{aligned} \quad (\text{S2})$$

where L is a Lipschitz constant. Similarly, we can also show,

$$\begin{aligned}\mathbb{E} \left[\left| \hat{\pi}(\hat{\mathbf{f}}(\mathbf{R}_i)) - \pi(\mathbf{f}(\mathbf{R}_i)) \right|^2 \right]^{1/2} &\leq L \cdot \mathbb{E} \left[\left\| \hat{\mathbf{f}}(\mathbf{R}_i) - \mathbf{f}(\mathbf{R}_i) \right\|^2 \right]^{1/2} + \mathbb{E} \left[\left| \hat{\pi}(\mathbf{f}(\mathbf{R}_i)) - \pi(\mathbf{f}(\mathbf{R}_i)) \right|^2 \right]^{1/2} \\ &\leq (L + 1) \delta_n n^{-1/4}.\end{aligned}\tag{S3}$$

Together with Assumption 7(b), Equation (S3) implies that there exists a sequence of positive constants δ'_n converging to zero as the sample size n increases such that the following inequality holds,

$$\mathbb{E} \left[\left| \hat{\pi}(\hat{\mathbf{f}}(\mathbf{R}_i)) - \pi(\mathbf{f}(\mathbf{R}_i)) \right|^2 \right]^{1/2} \cdot \mathbb{E} \left[\left| \hat{\mu}_{T_i}(\hat{\mathbf{f}}(\mathbf{R}_i)) - \mu_{T_i}(\mathbf{f}(\mathbf{R}_i)) \right|^2 \right]^{1/2} \leq \delta'_n n^{-1/2}.\tag{S4}$$

Thus, the standard regularity conditions of the DML theory (Chernozhukov et al., 2018) are satisfied for the estimated propensity score with the estimated deconfounder, i.e., $\hat{\pi}(\hat{\mathbf{f}}(\mathbf{R}_i))$. Finally, Assumptions 7(a)–(b) and Equations (S2) and (S4) imply,

$$\sqrt{n}(\hat{\tau} - \tau) \xrightarrow{d} \mathcal{N}(0, \sigma^2)$$

where $\sigma^2 = \mathbb{E}[\psi(\mathcal{D}_i; \tau, \mathbf{f}, \eta_1, \eta_0, \pi)^2]$.

□

S1.4 Proof of Theorem 3

Under a deep generative model (Definition 1), the distribution of \mathbf{X}_i only depends on \mathbf{P}_i , and hence we have $\{Y_i(\mathbf{x}), \tilde{T}_i(\mathbf{x})\} \perp\!\!\!\perp \mathbf{X}_i \mid \mathbf{P}_i$. Together with Assumption 2, Lemma 4.3 of Dawid (1979) implies $\{Y_i(\mathbf{x}), \tilde{T}_i(\mathbf{x})\} \perp\!\!\!\perp \mathbf{X}_i$. Under Assumptions 3, 4, 8, 9, and 10 (b), we have, for any $t, \tilde{t} \in \{0, 1\}$ and $\mathbf{u} \in \mathcal{U}$:

$$\{Y_i(\tilde{t}, \mathbf{u}), \tilde{T}_i(\tilde{t}, \mathbf{u})\} \perp\!\!\!\perp \{T_i, \mathbf{U}_i\}.\tag{S5}$$

Then, for any $\mathbf{u} \in \mathcal{U}$,

$$\begin{aligned}&\mathbb{E}[Y_i \mid T_i = 1, \mathbf{U}_i = \mathbf{u}] - \mathbb{E}[Y_i \mid T_i = 0, \mathbf{U}_i = \mathbf{u}] \\ &= \mathbb{E}[Y_i(\tilde{T}_i(1, \mathbf{u}), \mathbf{u}) \mid T_i = 1, \mathbf{U}_i = \mathbf{u}] - \mathbb{E}[Y_i(\tilde{T}_i(0, \mathbf{u}), \mathbf{u}) \mid T_i = 0, \mathbf{U}_i = \mathbf{u}] \\ &= \mathbb{E}[Y_i(\tilde{T}_i(1, \mathbf{u}), \mathbf{u}) - Y_i(\tilde{T}_i(0, \mathbf{u}), \mathbf{u})] \\ &= \mathbb{E}[Y_i(\tilde{T}_i(1, \mathbf{u}), \mathbf{u}) - Y_i(\tilde{T}_i(0, \mathbf{u}), \mathbf{u}) \mid \tilde{T}_i(1, \mathbf{u}) = 1, \tilde{T}_i(0, \mathbf{u}) = 0] \cdot \mathbb{P}(\tilde{T}_i(1, \mathbf{u}) = 1, \tilde{T}_i(0, \mathbf{u}) = 0) \\ &= \mathbb{E}[Y_i(1, \mathbf{u}) - Y_i(0, \mathbf{u}) \mid \tilde{T}_i(1, \mathbf{u}) = 1, \tilde{T}_i(0, \mathbf{u}) = 0] \cdot \mathbb{P}(\tilde{T}_i(1, \mathbf{u}) = 1, \tilde{T}_i(0, \mathbf{u}) = 0),\end{aligned}$$

where the second equality follows from Equation (S5), the third equality is due to Assumption 10. We also have:

$$\begin{aligned}\mathbb{P}(\tilde{T}_i(1, \mathbf{u}) = 1, \tilde{T}_i(0, \mathbf{u}) = 0) &= \mathbb{E}[\tilde{T}_i(1, \mathbf{u}) - \tilde{T}_i(0, \mathbf{u})] \\ &= \mathbb{E}[\tilde{T}_i(1, \mathbf{u}) \mid T_i = 1, \mathbf{U}_i = \mathbf{u}] - \mathbb{E}[\tilde{T}_i(0, \mathbf{u}) \mid T_i = 0, \mathbf{U}_i = \mathbf{u}] \\ &= \mathbb{E}[\tilde{T}_i \mid T_i = 1, \mathbf{U}_i = \mathbf{u}] - \mathbb{E}[\tilde{T}_i \mid T_i = 1, \mathbf{U}_i = \mathbf{u}]\end{aligned}$$

where the second equality follows from Equation (S5). Together, under Assumption 10 (a), we have:

$$\mathbb{E}[Y_i(1, \mathbf{u}) - Y_i(0, \mathbf{u}) \mid \tilde{T}_i(1, \mathbf{u}) = 1, \tilde{T}_i(0, \mathbf{u}) = 0] = \frac{\mathbb{E}[Y_i \mid T_i = 1, \mathbf{U}_i = \mathbf{u}] - \mathbb{E}[Y_i \mid T_i = 0, \mathbf{U}_i = \mathbf{u}]}{\mathbb{E}[\tilde{T}_i \mid T_i = 1, \mathbf{U}_i = \mathbf{u}] - \mathbb{E}[\tilde{T}_i \mid T_i = 1, \mathbf{U}_i = \mathbf{u}]}\tag{S6}$$

Finally, the LATE is identified as:

$$\begin{aligned}
& \mathbb{E}[Y_i(1, \mathbf{U}_i) - Y_i(0, \mathbf{U}_i) \mid \tilde{T}_i(1, \mathbf{U}_i) = 1, \tilde{T}_i(0, \mathbf{U}_i) = 0] \\
&= \int_{\mathcal{U}} \mathbb{E}[Y_i(1, \mathbf{U}_i) - Y_i(0, \mathbf{U}_i) \mid \tilde{T}_i(1, \mathbf{U}_i) = 1, \tilde{T}_i(0, \mathbf{U}_i) = 0, \mathbf{U}_i] dF(\mathbf{U}_i \mid \tilde{T}_i(1, \mathbf{U}_i) = 1, \tilde{T}_i(0, \mathbf{U}_i) = 0) \\
&= \int_{\mathcal{U}} \frac{\mathbb{E}[Y_i \mid T_i = 1, \mathbf{U}_i] - \mathbb{E}[Y_i \mid T_i = 0, \mathbf{U}_i]}{\mathbb{E}[\tilde{T}_i \mid T_i = 1, \mathbf{U}_i] - \mathbb{E}[\tilde{T}_i \mid T_i = 0, \mathbf{U}_i]} dF(\mathbf{U}_i \mid \tilde{T}_i(1, \mathbf{U}_i) > \tilde{T}_i(0, \mathbf{U}_i)) \\
&= \int_{\mathcal{U}} \frac{\mathbb{E}[Y_i \mid T_i = 1, \mathbf{U}_i] - \mathbb{E}[Y_i \mid T_i = 0, \mathbf{U}_i]}{\mathbb{E}[\tilde{T}_i \mid T_i = 1, \mathbf{U}_i] - \mathbb{E}[\tilde{T}_i \mid T_i = 0, \mathbf{U}_i]} \cdot \frac{\mathbb{P}(\tilde{T}_i(1, \mathbf{U}_i) = 1, \tilde{T}_i(0, \mathbf{U}_i) = 0 \mid \mathbf{U}_i)}{\mathbb{P}(\tilde{T}_i(1, \mathbf{U}_i) = 1, \tilde{T}_i(0, \mathbf{U}_i) = 0)} dF(\mathbf{U}_i) \\
&= \int_{\mathcal{U}} \frac{\mathbb{E}[Y_i \mid T_i = 1, \mathbf{U}_i] - \mathbb{E}[Y_i \mid T_i = 0, \mathbf{U}_i]}{\mathbb{E}[\tilde{T}_i \mid T_i = 1, \mathbf{U}_i] - \mathbb{E}[\tilde{T}_i \mid T_i = 0, \mathbf{U}_i]} \cdot \frac{\mathbb{E}[\tilde{T}_i \mid T_i = 1, \mathbf{U}_i] - \mathbb{E}[\tilde{T}_i \mid T_i = 0, \mathbf{U}_i]}{\mathbb{P}(\tilde{T}_i(1, \mathbf{U}_i) = 1, \tilde{T}_i(0, \mathbf{U}_i) = 0)} dF(\mathbf{U}_i) \\
&= \frac{\int_{\mathcal{U}} \mathbb{E}[Y_i \mid T_i = 1, \mathbf{U}_i] - \mathbb{E}[Y_i \mid T_i = 0, \mathbf{U}_i] dF(\mathbf{U}_i)}{\int_{\mathcal{U}} \mathbb{E}[\tilde{T}_i \mid T_i = 1, \mathbf{U}_i] - \mathbb{E}[\tilde{T}_i \mid T_i = 0, \mathbf{U}_i] dF(\mathbf{U}_i)} \\
&= \frac{\int_{\mathbb{R}^r} \mathbb{E}[Y_i \mid T_i = 1, \mathbf{f}(\mathbf{R}_i)] - \mathbb{E}[Y_i \mid T_i = 0, \mathbf{f}(\mathbf{R}_i)] dF(\mathbf{R}_i)}{\int_{\mathbb{R}^r} \mathbb{E}[\tilde{T}_i \mid T_i = 1, \mathbf{f}(\mathbf{R}_i)] - \mathbb{E}[\tilde{T}_i \mid T_i = 0, \mathbf{f}(\mathbf{R}_i)] dF(\mathbf{R}_i)}
\end{aligned}$$

where the second equality follows from Equation (S6), the third equality is due to Bayes' theorem, and the last equality (as well as the existence of deconfounder) follows from the same argument used to establish Theorem 1. \square

S2 Results of Additional Simulation Studies

	Bias	RMSE	95% confidence interval		Runtime
			coverage	avg. length	(seconds)
Weak confounding w/ separability					
Proposed estimator (new)	-0.33	1.06	0.94	3.47	42.1
Proposed estimator (reuse)	-0.26	0.98	0.92	2.95	54.1
Difference-in-Means	3.61	3.61	0	4.72	0.0
T-learner with BERT	1.17	1.00	0.12	0.53	296
DR-learner with BERT	0.58	4.21	0.93	2.10	327
Moderate confounding w/ separability					
Proposed estimator (new)	-1.07	2.72	0.95	9.00	43.6
Proposed estimator (reuse)	-1.05	2.36	0.93	6.85	62.9
Difference-in-Means	7.95	7.95	0	9.50	0.0
T-learner with BERT	3.44	2.27	0.05	0.92	673
DR-learner with BERT	2.09	18.3	0.92	5.14	720
Strong confounding w/ separability					
Proposed estimator (new)	-14.6	36.9	0.88	113	55.3
Proposed estimator (reuse)	-15.1	36.0	0.92	96.3	74.3
Difference-in-Means	86.0	86.0	0	95.7	0.0
T-learner with BERT	112	114	0	13.2	2731
DR-learner with BERT	208	917	0.26	382	2756
Weak confounding w/o separability					
Proposed estimator (new)	3.23	3.27	0	1.45	35.9
Proposed estimator (reuse)	2.87	2.89	0	1.34	41.1
Difference-in-Means	2.20	2.20	0.03	4.03	0.0
T-learner with BERT	2.55	2.70	0.01	1.02	320
DR-learner with BERT	6.18	16.7	0.05	4.69	348
Moderate confounding w/o separability					
Proposed estimator (new)	6.70	6.76	0	2.89	42.5
Proposed estimator (reuse)	5.90	5.93	0	2.66	44.9
Difference-in-Means	4.39	4.40	0	8.04	0.0
T-learner with BERT	7.56	7.66	0	1.85	624
DR-learner with BERT	12.1	30.5	0.06	10.1	656
Strong confounding w/o separability					
Proposed estimator (new)	76.3	76.7	0	29.8	53.0
Proposed estimator (reuse)	66.8	67.1	0	27.7	56.4
Difference-in-Means	44.0	44.0	0	80.3	0.0
T-learner with BERT	116	117	0	13.2	2689
DR-learner with BERT	207	814	0.26	425	2716

Table S1: Simulation Results with 200 Monte Carlo trials

	Bias	RMSE	95% confidence interval coverage	avg. length	Average time (sec.)
Weak confounding w/ separability					
Proposed estimator (new)	-0.31	1.09	0.93	3.55	43.0
Proposed estimator (reuse)	-0.21	0.96	0.93	2.90	55.7
Moderate confounding w/ separability					
Proposed estimator (new)	-0.99	2.77	0.92	8.83	45.7
Proposed estimator (reuse)	-1.00	2.67	0.90	6.99	61.7
Strong confounding w/ separability					
Proposed estimator (new)	-14.3	36.1	0.89	108	57.7
Proposed estimator (reuse)	-16.0	38.1	0.90	98.8	76.3

Table S2: Simulation Results based on 1000 Monte Carlo trials